NASA Technical Memorandum 81901

NONLINEAR DYNAMIC RESPONSE OF A UNI-DIRECTIONAL MODEL FOR THE TILE/PAD SPACE SHUTTLE THERMAL PROTECTION SYSTEM

J. M. HOUSNER, H. H. EDIGHOFFER, AND K. C. PARK

NOVEMBER 1980

National Aeronautics and Space Administration

Langley Research Center
Hampton, Virginia 23665

NONLINEAR DYNAMIC RESPONSE OF A UNI-DIRECTIONAL MODEL FOR THE TILE/PAD SPACE SHUTTLE THERMAL PROTECTION SYSTEM

By Jerrold M. Housner, Harold H. Edighoffer, and K. C. Park

SUMMARY

A uni-directional analysis of the nonlinear dynamic behavior of the space shuttle tile/pad thermal protection system is developed and examined for imposed sinusoidal and random motions of the shuttle skin and/or applied tile pressure. The analysis accounts for the highly nonlinear stiffening hysteresis and viscous behavior of the pad which joins the tile to the shuttle skin. Where available, experimental data are used to confirm the validity of the analysis. Both analytical and experimental studies reveal that the system resonant frequency is very high for low amplitude oscillations but decreases rapidly to a minimum value with increasing amplitude. Analytical studies indicate that with still higher amplitude the resonant frequency increases slowly. The nonlinear pad is also responsible for the analytically and experimentally observed distorted response wave shapes having high sharp peaks when the system is subject to sinusoidal loads. Furthermore, energy dissipation in the pad is studied analytically and it is found that the energy dissipated is sufficiently high to cause rapid decay of dynamic transients. Nevertheless, the sharp peaked nonlinear responses of the system lead to higher magnification factors than would be expected in such a highly damped linear system.

INTRODUCTION

The space shuttle orbiter thermal protection system consists of ceramic tiles bonded to thin nylon felt pads, known as strain isolator pads, which are composed of thousands of intertwined nylon filaments. The pads, in turn, are bonded to the aluminum skin (substrate) of the shuttle orbiter.

During a mission, tile/pad combinations experience dynamic loads arising from acoustics, structural vibration, and transonic shock. As a consequence, the pad experiences many cycles of loading of varying magnitudes. Experiments such as those described in reference 1 have shown that as the pad is cyclically loaded and unloaded, hysteresis loops occur in a stress strain characterization of the material. Furthermore, these loops creep as a function of stress level and number of cycles. The creep of the loops eventually becomes very small with each additional cycle, but its effect is to produce a highly nonlinear hardening pad material which is quite soft at low stress levels and considerably stiffer at higher stress levels. As shown in reference 2, for tiles under static loads, the nonlinear pad material properties after cycling significantly affected tile/pad behavior, producing in many cases considerably higher tile/pad through-the-thickness interface stresses than before cycling. The nonlinear pad properties can also be expected to significantly affect the response of the system under dynamic loads.

For a large class of tile/pad combinations (those for which the tile and pad centroids lie along a line normal to the tile surface), a single-degree-of-freedom model of the system is sufficient to characterize the response of the system under uniform applied dynamic pressure or motion. Such a model can predict dynamic tile/pad through-the-thickness interface stresses which are known to be critical to the integrity of the system.

The purpose of this paper is to present the development, verification, and application of an analysis for predicting the nonlinear single-degree-of-freedom response of the tile/pad/substrate thermal protection system to sinusoidal and random applied pressure on the tile and/or imposed motion of the substrate.

Inasmuch as the mathematical modeling of the pad material is critical to the analysis, the modeling will be discussed including the following: assumptions; modeling of the observed stress-strain behavior; damping law development; and effective percent of critical damping. Verification of the analysis is accomplished through comparison with experiment where available. In addition, results for the following will be presented:

(1) Variation of resonant frequency with amplitude of imposed sinusoidal substrate acceleration and applied tile pressure

(2) Variation of magnification factor with amplitude of imposed sinusoidal substrate acceleration and applied tile pressure

(3) Response to random substrate motion.

MATHEMATICAL MODELING OF THE SPACE SHUTTLE TILE/PAD THERMAL PROTECTION SYSTEM

General Discussion

As shown in figure 1, the space shuttle tile/pad thermal protection system consists of ceramic tiles bonded to the space shuttle through a nylon felt pad. In deriving a mathematical model for the system several assumptions are made. For the tile itself, it is assumed, as in reference 2, that

Assumption (1): Each tile behaves as a rigid body.

For the pad, which has a complex nonlinear material behavior simplifying assumptions are made based upon observations of its behavior under cyclic load.

Conditioning of the Pad Under Slow Cyclic Load

Material property tests such as those of reference 1 revealed, as displayed in figure 2, that under slow cyclic loading of a prescribed amplitude the pad exhibits hysteretic behavior. The hysteresis loops thus formed creep as a function of load amplitude and number of cycles. However, it is observed that

the creep of the loop eventually becomes very small with additional load cycles of the same or lower amplitude. This process which produces a quasi-stabilized material will be referred to as "conditioning." Provided the pad has not experienced a load amplitude higher than the one conditioned at, it would appear that the creep of the hysteresis loops can be safely neglected during a short time analysis. Hence,

Assumption (2): It is assumed that the pad material has been conditioned at a load amplitude which is not exceeded during the period of time to be analyzed.

Analytical responses of the system have indicated that the system is not sensitive to small additional creeping. As a consequence of Assumption (2), the analysis may be carried out over a short period of time (e.g., a few hundred cycles) and then restarted using material data corresponding to additional cycles at the calculated stress amplitudes which meet or exceed the "conditioning" amplitude.

Pad Through-the-Thickness Stress

For reasons discussed later in this section, it is assumed that

Assumption (3): The total through-the-thickness pad stress is the algebraic sum of strain-rate independent and strain-rate dependent stresses denoted as σ_s and σ_D, respectively, so that the total pad stress is

$$\sigma = \sigma_s + \sigma_D \tag{1}$$

Strain-rate independent pad stresses, σ_s.- It can be observed in figure 2 that the slow load-rate hysteretic conditioned loop involves irrecoverable and recoverable deformations. The sharply pointed character of the loop indicates the presence of static coulomb frictional damping which is strain-rate independent. This is physically reasonable since filaments are sliding over one another during loading or unloading. It is, therefore, assumed that

Assumption (4): The slow load-rate experimental curves account for all strain-rate independent stresses, σ_s, in the pad, both elastic and inelastic.

Figure 3 illustrates typical loading/unloading paths from different strain-rate independent states (σ_s, ε) within and on the conditioned loop envelope, where ε is the through-the-thickness pad strain.

Based on the observation of pad behavior similar to that exhibited in figure 3 and as a consequence of Assumption (2), it is further assumed that

Assumption (5): Irrespective of loading or unloading path, the pad strain-rate independent state (σ_s, ε) cannot lie outside of the conditioned path hysteretic loop envelope.

Within the envelope, it is assumed that

Assumption (6): Loading/unloading paths may be curve fitted approximately by appropriate scaling and translation of portions of the envelope.

This assumption is reasonable since the envelope itself is composed of a loading and unloading path between the extrema of the conditioning cycle. Details on the curve fitting are given in Appendix A.

Strain-rate dependent pad stresses, σ_D.- It is known (see, for example, ref. 3), that for a driven linear spring/mass system, the energy dissipation due to coulomb strain-rate independent damping is not sufficient to produce bounded oscillations at resonant frequencies. Inasmuch as physical oscillations are always bounded, it would appear reasonable to postulate that an additional energy dissipation mechanism which is strain-rate dependent is present in the pad. Indeed, dynamic tests indicate that this is the case.

It is assumed that the strain-rate dependent stress, σ_D, is given by a power law† namely,

Assumption (7): $$\sigma_D = \frac{2m\Omega_r\zeta}{A_p}(h_p\dot{\varepsilon})\left|\frac{2\pi\dot{\varepsilon}}{\Omega_r}\right|^{q-1} \tag{2}$$

In equation (2), $\dot{\varepsilon}$ is the pad through-the-thickness (z-direction) strain rate, m is the tile mass, h_p is the pad conditioned thickness, A_p is the tile/pad contact area, Ω_r is a reference frequency, and ζ, q are damping parameters to be determined from experiment. A single term representation of σ_D is used rather than a sum of such terms since it is highly desirable to keep the number of parameters to be validated from tests to a minimum. The evaluation of these parameters is considered in a subsequent section. The existence of σ_D allows the total stress-strain state (σ, ε) to lie outside the envelope.

Integration of the Equation of Motion

Equilibrium of the tile in the z-direction is satisfied provided

$$m\ddot{w} + A_p(\sigma_s + \sigma_D) = P(t) \tag{3}$$

where $\ddot{w}$ is the tile acceleration in the positive z-direction, P is the applied tile transient load, σ_D is given by equation (2), and σ_s is provided by tracing out the loading/unloading path which depends upon prior stress-strain history where the pad strain is given by

†Examination of such power damping laws in otherwise linear systems is contained, for example, in reference 4.

$$\varepsilon = (w - w_s)/h_p \tag{4}$$

in which w and w_s are the transient displacements of the tile and substrate, respectively, in the positive z-direction.

Equation (3) is integrated explicitly by using the following recursive algorithms at the ith time step:

$$\dot{w}_{i+1} = \dot{w}_i + \Delta t\left[P_i - A_p\left(\sigma_{s_i} + \sigma_{D_i}\right)\right]\Big/m \tag{5}$$

$$w_{i+1} = w_i + \Delta t\ \dot{w}_{i+1} \tag{6}$$

where $(\cdot)$ over any quantity indicates differentiation with respect to time and Δt is an appropriate time step. The initial conditions for equation (3) may be specified on σ_s, ε, and $\dot{\varepsilon}$. If the initial state of (σ,ε) lies outside the envelope, then $\dot{\varepsilon}$ must initially be nonzero.

Selection of Strain-Rate Dependent Damping Parameters

General discussion.- In a linear spring-mass-dashpot system, the response amplitude due to sinusoidal oscillations of the base is significantly affected by the viscous damping coefficient whereas the resonant frequency is not as strongly influenced by the damping coefficient. This is also generally true of nonlinear systems except that in addition, the amplitude and resonant frequency have a nonlinear dependence on the imposed substrate motion or applied tile pressure. In order to evaluate the two damping parameters of equation (2) it seems appropriate to select these based upon a comparison of analytical and experimental response amplitudes due to imposed sinusoidal motions of the substrate or applied tile pressure oscillations at the resonant frequency of the system. Inasmuch as it is anticipated that the majority of pad stress on the space shuttle will be due to substrate motion, the damping parameters are based on experimental correlation for imposed sinusoidal substrate motion, where the experimental results are presented in references 5 and 6. Once the parameters are selected, the system response under sinusoidal applied tile pressure and random substrate motion are examined.

Sinusoidal substrate motion.- Consider the case of $P = 0$ and an imposed sinusoidal substrate motion given by

$$w_s = \frac{\alpha G}{\Omega^2} \sin \Omega t \tag{7}$$

where α is a prescribed amplitude, G is the acceleration of gravity (e.g., if w_s is in inches, G is 386 in/sec^2), and Ω is the imposed circular frequency.

The resonant frequency, Ω_o, is taken as that value of Ω which yields the peak amplitude response (resonant amplitude) occurring over the frequency range of interest (usually 0 to 1000 Hz). Figure 4 illustrates a typical variation with Ω of response amplitude expressed as magnification factor f_s, where

$$f_s = \ddot{w}/\alpha G \tag{8}$$

For a square LI 900 15.24 × 15.24 × 9.525 cm tile on a 12.7 × 12.7 × 0.406 cm pad (6 × 6 × 3.75 in. tile on a 5 × 5 × 0.160 in. pad), figures 5, 6, and 7 present families of analytical curves which show the variations of resonant magnification factors with α for different selections of the damping parameters ζ and q. The figures serve to show the effect of each parameter on the shape of the curves. Available experimental values are also displayed. Within realistic limits it appears that an appropriate selection of the parameters is

$$\zeta = 0.15, \quad q = 2 \tag{9}$$

where the reference frequency, Ω_r, is 100 Hz.

This selection is guided by the following considerations:

(1) The results displayed in the figures indicate that irrespective of q a value of ζ can be found such that the experimental data scatter is reasonably approximated. Hence for $q = 1$, $\zeta \simeq 0.2$; for $q = 2$, $\zeta \simeq 0.15$; for $q = 3$, $\zeta \simeq 0.06$.

(2) The lowest integer exponential damping law which fits the data scatter should be selected; however, at present, experimental data are available only for $\alpha \leq 35$.

(3) In the absence of available experimental data, a criterion for $\alpha > 35$ is required to make a reasonable selection for q. This criterion is taken to be that f_s must remain bounded as α goes to infinity, in particular

$$f_s < (f_s)_{max} \tag{10}$$

where $(f_s)_{max}$ is chosen to be the maximum value of f_s observed among the available experimental data.

(4) The criterion of equation (10) eliminates $q = 1$, a linear viscous damper, as a selection since f_s for values of ζ, which pass through the data scatter at $\alpha \leq 35$, increases above $(f_s)_{max}$ as α increases.

(5) The lowest integer exponential damping law which produces a good data fit at $\alpha \leq 35$ and satisfies equation (10) has q and ζ as prescribed by equation (9).

(6) Additional experimental data for $\alpha > 35$ are required to determine a better selection.

COMPUTER CODE

A computer code which solves equation (1) using the time integration algorithm of equations (5) and (6) has been developed. The code traces out the loading/unloading curves which are approximated according to the relations presented in Appendix A. Relevant response quantities such as pad stress and strain, tile and substrate accelerations are output. A short user's guide to the code is provided in Appendix B.

APPLICATIONS

Sinusoidal Substrate Motion

Figure 6 provides the variation of the magnification factor, f_s, with substrate acceleration, α, at the resonant frequency for a LI 900 15.24 × 15.24 × 9.525 cm tile on a 12.7 × 12.7 × 0.406 cm pad (6 × 6 × 3.75 in. tile on a 5 × 5 × 0.160 in. pad). The calculated resonant frequency variation with α is given in figure 8 along with corresponding experimental results. Agreement is good, with both analysis and experiment exhibiting similar trends.

With increasing substrate amplitude of motion, analysis and experiment show a rapid decrease in frequency (effective dynamic softening) followed by a slow increase in frequency (effective dynamic hardening). The trend can be understood by considering the material behavior of figure 3. At low amplitude, the material follows a stiff loading/unloading loop (loop A), with little or no portion of it on the low modulus region. This indicates that for low level oscillations the friction force between fibers accounts for the entire load carrying pad mechanism. As the amplitude is increased, a larger portion of the loop contains the low modulus region (loop B), and so the frequency decreases. With further increase in amplitude, the frequency starts increasing again as portions of the loop begin to include the higher modulus region at raised stress levels (loop C).

Examination of the analytically predicted and experimentally observed steady state tile/pad interface stress, σ, as a function of time reveals the highly nonlinear nature of the response. Figure 9 shows $\sigma(t)$ near the resonant frequency when $\alpha = 30$. The agreement between results from analysis and test is very good; both show a highly nonlinear response with a sharp stress peak. (A linear analysis would give a purely sinusoidal response.) The peaks seem to be due to the tile acquiring a high velocity during its travel over the soft material range which causes it to overshoot into the stiff material range thus producing high stresses which result in the high magnification factors of figures 5 to 7.

Random Substrate Motion

Consider again the case of a LI 900 15.24 × 15.24 × 9.525 cm tile on a 12.7 × 12.7 × 0.406 cm pad (6 × 6 × 3.75 in. tile on a 5 × 5 × 0.160 in. pad), where the substrate undergoes random accelerations. Figure 10 presents a time slice of the random substrate motion, analytical tile response, and experimental tile response where the random substrate motion has the power spectral density given in figure 11. Correlation between experiment and analysis is good in spite of the variability which exists in pad properties from specimen to specimen.

Applied Sinusoidal Tile Pressure

Using the values of ζ and q established on the basis of imposed sinusoidal substrate motion, the system response to sinusoidally varying applied tile pressure

$$P = p_1 A_T + p_2 A_T \sin \omega t \tag{11}$$

is examined for a LI 900 15.24 × 15.24 × 9.525 cm tile on a 12.7 × 12.7 × 0.406 cm pad (6 × 6 × 3.75 in. tile on a 5 × 5 × 0.160 in. pad) where A_T is the tile surface area and ω is the circular frequency. Figures 12 and 13 illustrate the response of the system when $p_1 = 0$. In figure 12 the variation of resonant frequency with magnitude of p_2 is presented while figure 13 shows the variation of magnification factor, f_p, with magnitude of p_2. In the case of applied tile pressure, f_p is defined as

$$f_p = \sigma/(p_1 + p_2) \tag{12}$$

It is evident from a comparison of these figures with figures 5 to 8 that the response trends with both sinusoidal substrate and tile pressure excitation are similar.

Application of Analysis To Determine Effective Pad Damping Properties

General discussion.- It has been shown herein that the tile/pad system is highly nonlinear. Nevertheless, it may be desirable to establish linear models which can provide reasonable results for certain dynamic characteristics of the system. To this end, an equivalent linear damper is sought by using the nonlinear analysis to evaluate an equivalent linear percent of critical damping for the pad.

Five procedures are employed to evaluate the pad percent of critical damping. It is shown that different values result depending on the procedure

employed. However, for the present need of evaluating pad stresses, a procedure based upon stress magnification factor appears to be most suitable.

Before proceeding with the evaluation, it is useful to review some basic linear behavior results associated with base driven, force drive, and free oscillations of the system.

Linear system.- The response of a linear spring/mass/dashpot system with spring and dashpot in parallel is well understood. The damping force is proportional to $\dot{\varepsilon}$ and the critical damping coefficient is defined as

$$c_{cr} = 2m\omega_o \tag{13}$$

where ω_o is the resonant frequency without the dashpot.

Case of an imposed sinusoidal substrate motion: For the case of an imposed sinusoidal substrate motion, the magnitude of the mass (tile) motion is given by

$$|w| = f_s|w_s| \tag{14}$$

where f_s near resonance may be approximated by

$$f_s \simeq \frac{1}{2\xi}\sqrt{1 + 4\xi^2} \tag{15}$$

in which ξ is the critical damping ratio given by

$$\xi = \frac{c}{c_{cr}} = \frac{c}{2m\omega_o} \tag{16}$$

The energy dissipated per cycle, E_D, in the case of the sinusoidally substrate driven system is given by

$$\frac{E_D}{4\pi E_K} = \xi\left(1 - \frac{1}{f_s{}^2}\right) \tag{17}$$

where

$$E_K = \frac{1}{2} m\omega_o{}^2|w|^2 \tag{18}$$

is the maximum kinetic energy of the mass during any cycle, and f_s is given by equation (15).

Case of an applied tile pressure: For the case of an applied tile pressure, the magnitude of the mass motion is given by

$$|w| = f_p|P|/k \tag{19}$$

where k is the linear spring stiffness constant and f_p near resonance may be approximated by

$$f_p = \frac{1}{2\xi} \tag{20}$$

The energy dissipated per cycle in the case of the sinusoidally force driven system is given by

$$\frac{E_D}{4\pi E_K} = \xi \tag{21}$$

where E_K is given by equation (18).

Case of a force free system: For the case of a force free system, in which the mass is given an initial displacement and allowed to decay exponentially to zero displacement, the critical damping is given by the "log decrement" as

$$\xi = -\frac{1}{2\pi} \ln\left(w_{t=T}/w_{t=0}\right) \tag{22}$$

where

$$T = 2\pi/\omega_o \tag{23}$$

is the response period.

Nonlinear system.- For the nonlinear tile/pad system, equivalent values of ξ are calculated on the basis of the following five procedures:

(1) Magnification factor in substrate driven system

(2) Energy dissipation in substrate driven system

(3) Magnification factor in tile pressure driven system

(4) Energy dissipation in tile pressure driven system

(5) Log decrement

where ξ_i denotes a value based on the ith procedure. In a linear system, ξ_i would be independent of force or base acceleration magnitude and be the same for all five procedures. However, in the nonlinear pad/tile system, this is not the case.

Consider the case of a LI 900 15.24 × 15.24 × 9.525 cm tile on a 12.7 × 12.7 × 0.406 cm pad (6 × 6 × 3.75 in. tile on a 5 × 5 × 0.160 in. pad). In figure 14, ξ_1 and ξ_2 are shown for this case where ξ_1 is found from equation (15) and the results of figure 6 with $\zeta = 0.15$ and $q = 2$ while ξ_2 is found from equation (17) where E_D is calculated by the formula

$$E_D = \int_{t_o}^{t_o+T} A_p \sigma(\dot{w} - \dot{w}_s)dt \tag{24}$$

in which t_o is any time large enough so that the system response is in a steady-state condition, $\dot{w}$ and σ are provided by the numerical solution of equation (3), and $\dot{w}_s$ from the differentiation of equation (7).

The results indicate that except for low substrate accelerations, procedures (1) and (2) give nearly identical results of about 16 to 18 percent of critical damping for moderate to high substrate accelerations. At low acceleration levels, it would be best to use ξ_1, inasmuch as magnification factors are of critical importance to the integrity of the system.

The results for ξ_3 and ξ_4 are given in figure 15 where the value of ξ_3 is calculated using equation (20) and figure 12 while ξ_4 is found from equation (21). Unlike the substrate driven system, the pressure driven system results in vastly different critical damping ratios between procedures (3) and (4), based on magnification factor and energy dissipation, respectively, for all amplitudes of oscillating pressure. Moreover, neither procedure (3) nor (4) agrees well with (1) or (2). Procedure (3) results in damping ratios smaller than those of procedure (1) since the magnification factors under applied sinusoidal pressure are larger than those under applied substrate motion. On the other hand, procedures (2) and (4) give comparable values for peak critical damping ratios, but procedure (4) does not result in the drop off of the damping ratio seen in procedure (2) for increasing input energy.

The results of ξ_5 are given in figure 16 where the analysis has been used in conjunction with equation (22). Procedure (5) results in a monotonically increasing critical damping ratio with increasing initial strain and thus yields values seen in all the other four procedures. Use of equation (22) implies a full cycle determination of log decrement whereas reference 4 suggests the use of a half cycle determination when $q > 1$. However, since the pad properties lead to generally larger responses on the tensile half cycle than the compressive half cycle even when there is no viscous damping, a half cycle determination would produce misleading results whereas a full cycle determination would not.

Two conclusions are drawn from the comparison of these five procedures. First, the system is too nonlinear to permit an equivalent linearized damping

evaluation that allows for all possible situations. The nonlinear behavior gives rise to high stress peaks and thus high magnification factors even in the presence of considerable energy losses due to pad dissipation mechanisms. Second, if a linearized model is desired, the critical damping ratio should be chosen so as to correlate with the nonlinear results which are of interest to the analyst. In the case of the space shuttle, this implies using about 16 percent or 10 percent critical damping for imposed substrate motion or applied tile pressure, respectively. These numbers are based on magnification factors, procedures (1) and (3), respectively.

Energy dissipation due to friction alone.- By taking the damping parameter, ζ, equal to zero, the energy dissipated per cycle as a consequence of strain-rate independent frictional mechanism in the pad may be examined. This is shown in figure 17 for imposed sinusoidal substrate acceleration. Comparison with the results of procedure (2) in figure 14 indicates that the energy loss due to friction alone is about 25 to 30 percent of the total energy loss with the remainder of the loss due to nonlinear viscous damping.

CONCLUDING REMARKS

A uni-directional nonlinear dynamic analysis and associated computer code for the space shuttle tile/pad thermal protection system have been developed and examined for imposed sinusoidal and random motions of the substrate and/or applied tile pressure. The analysis accounts for the nonlinear stiffening, hysteresis, and viscous behavior of the pad material and is in reasonably good agreement with experiment for resonant frequency and response magnification under imposed sinusoidal substrate motion as well as imposed random substrate motion. Application of the analysis reveals a highly nonlinearly behaving system whose resonant frequency is very high (over 500 Hz) for low amplitude oscillations, but rapidly decreases to a minimum value with increasing amplitude from which it increases slowly with further increase in amplitude. The nonlinear pad also causes distorted response wave shapes having high stress peaks when the system is subject to sinusoidal loads. Furthermore, energy dissipation in the pad per cycle leads to relatively high "log decrement" damping and thus rapid decay of dynamic transients. Nevertheless, the sharp peaked nonlinear responses lead to higher magnification factors based on peak responses than would be expected in an equivalent highly damped linear system.

APPENDIX A

CURVE FIT OF PAD MATERIAL PROPERTIES

Conditioned Envelope

As a consequence of assumptions (5) and (6) in the main body of the paper, a curve fit of the conditioned hysteretic loop is first sought. To this end the envelope is divided into six segments labeled sequentially in figure 18. Segments (1) and (2) are straight lines whose equations are defined in terms of measured values indicated in figure 18 as

$$\sigma_{s1} = \bar{\sigma}_b + E_z\varepsilon \tag{A1}$$

$$\sigma_{s2} = \bar{\sigma}_a + E_z\varepsilon \tag{A2}$$

Parts (3) to (6) are defined by fifth order polynomials as

$$\sigma_{si} = C_{i0} + C_{i1}(\varepsilon - \bar{\varepsilon}_{i1}) + C_{i3}(\varepsilon - \bar{\varepsilon}_{i1})^3 + C_{i5}(\varepsilon - \varepsilon_{i1})^5; \quad i = 3,4,5,6 \tag{A3}$$

where the four coefficients for the ith curve are chosen such that the ith curve passes through the measured points of $(\bar{\sigma}_{ij}, \bar{\varepsilon}_{ij})$, $j = 1,2,3$, on part (i) of the envelope and has a slope equal to E_z at $(\bar{\sigma}_{i1}, \bar{\varepsilon}_{i1})$. Since parts (4) and (5), and (3) and (6) join at their respective end points,

$$\bar{\sigma}_{43} = \bar{\sigma}_{53}; \quad \bar{\varepsilon}_{43} = \bar{\varepsilon}_{53}; \quad \bar{\sigma}_{33} = \bar{\sigma}_{63}; \quad \bar{\varepsilon}_{33} = \bar{\varepsilon}_{63} \tag{A4}$$

and E_z is given by

$$E_z = (\bar{\sigma}_{51} - \bar{\sigma}_{31})/(\bar{\varepsilon}_{51} - \bar{\varepsilon}_{31}) \tag{A5}$$

while $\bar{\sigma}_a$ and $\bar{\sigma}_b$ are given by

$$\bar{\sigma}_a = \bar{\sigma}_{61} - E_z\bar{\varepsilon}_{61}$$

$$\bar{\sigma}_b = \bar{\sigma}_{31} - E_z\bar{\varepsilon}_{31} \tag{A6}$$

and

$$\frac{\bar{\sigma}_{41} - \bar{\sigma}_{61}}{\bar{\varepsilon}_{41} - \bar{\varepsilon}_{61}} = \frac{\bar{\sigma}_{51} - \bar{\sigma}_{31}}{\bar{\varepsilon}_{51} - \bar{\varepsilon}_{31}} \tag{A7}$$

Consequently, nineteen independently measured points are required to characterize the envelope curve fit used herein.

The coefficients of equation (A3) may now be determined as

$$C_{i0} = \bar{\sigma}_{i1}$$

$$C_{i1} = E_z \tag{A8}$$

and

$$\begin{Bmatrix} C_{i3} \\ C_{i5} \end{Bmatrix} = \begin{bmatrix} (\bar{\varepsilon}_{i2} - \bar{\varepsilon}_{i1})^3 & (\bar{\varepsilon}_{i2} - \bar{\varepsilon}_{i1})^5 \\ (\bar{\varepsilon}_{i3} - \bar{\varepsilon}_{i1})^3 & (\bar{\varepsilon}_{i3} - \bar{\varepsilon}_{i1})^5 \end{bmatrix}^{-1} \begin{Bmatrix} \bar{\sigma}_{i2} - \bar{\sigma}_{i1} - E_z\bar{\varepsilon}_{i1} \\ \bar{\sigma}_{i3} - \bar{\sigma}_{i1} - E_z\bar{\varepsilon}_{i1} \end{Bmatrix} \tag{A9}$$

Paths Within the Envelope

General discussion.- With the envelope defined by equations (A1) to (A3), the constraint associated with assumption (5) can be met. Paths within the envelope by assumption (6) follow trajectories similar to the envelope itself. These trajectories are designated as positive or negative paths depending on whether the strain rate, $\dot{\varepsilon}$, is positive or negative along the path. For example, on the envelope, paths (1), (3), and (5) are positive whereas (2), (4), and (6) are negative. Paths within the envelope are determined by the state of stress-strain existing when $\dot{\varepsilon}$ changes sign. The approximations to the positive and negative paths are now described.

Positive paths.- Positive paths within the envelope are generally approximated by a curved portion, or a straight portion, depending on whether the reversal strain $\bar{\varepsilon}_A$ when $\dot{\varepsilon}$ last changed sign from negative to positive is less than or greater than the upper cutoff strain, $\bar{\varepsilon}_U$. However, when a positive interior path intersects a positive envelope path, the envelope path is followed.

Reversal strain less than upper cutoff strain: When the reversal strain, $\bar{\varepsilon}_A$, is less than the upper cutoff strain, $\bar{\varepsilon}_U$, the positive path is approximated by a fifth order polynomial similar to segment (3) but passing through three points designated as A, B, and C and with slope E_z at point C. The state of stress-strain at these points is as follows:

Point A has the state of stress-strain $(\bar{\sigma}_A, \bar{\varepsilon}_A)$ at which $\dot{\varepsilon}$ changes sign from negative to positive.

Point B has the state of stress-strain $(\bar{\sigma}_B, \bar{\varepsilon}_B)$ proportioned from the envelope curve (3) and given by

$$\bar{\sigma}_B = \bar{\sigma}_B^* - \hat{\varepsilon}_{32} E_z$$

$$\bar{\varepsilon}_B = \bar{\varepsilon}_A - \hat{\varepsilon}_{32} \tag{A10}$$

where

$$\bar{\sigma}_B^* = \bar{\sigma}_C^* + \frac{\bar{\sigma}_{B_P} - \bar{\sigma}_{C_P}}{\bar{\sigma}_{33} - \bar{\sigma}_{C_P}} (\bar{\sigma}_A - \bar{\sigma}_C^*)$$

$$\bar{\sigma}_C^* = \bar{\sigma}_{31} + (\bar{\varepsilon}_A - \bar{\varepsilon}_{31}) E_z$$

$$\bar{\sigma}_{B_P} = \bar{\sigma}_{32} + \hat{\varepsilon}_{32} E_z$$

$$\bar{\sigma}_{C_P} = \bar{\sigma}_{31} + \hat{\varepsilon}_{31} E_z$$

$$\hat{\varepsilon}_{31} = \gamma(\bar{\varepsilon}_{33} - \bar{\varepsilon}_{31})$$

$$\hat{\varepsilon}_{32} = \gamma(\varepsilon_{33} - \varepsilon_{32}) \tag{A11}$$

Point C has the state of stress-strain $(\sigma_C, \bar{\varepsilon}_C)$ given by

$$\bar{\sigma}_C = \bar{\sigma}_{31} + (\bar{\varepsilon}_A - \bar{\varepsilon}_{31}) E_z - \hat{\varepsilon}_{31} E_z$$

$$\bar{\varepsilon}_C = \bar{\varepsilon}_A - \hat{\varepsilon}_{31} \tag{A12}$$

The factor $\gamma \leq 1$ is introduced because the paths at low stress levels cannot be accurately determined from test due to the very soft nature of a low stressed pad. Its value is

$$\gamma = \gamma_1^{(1-r)}; \quad \bar{\varepsilon}_{61} \leq \bar{\varepsilon}_A \leq \bar{\varepsilon}_{51} \tag{A13}$$

where

$$r = \left| \frac{\bar{\sigma}_A}{\bar{\varepsilon}_A E_z + \bar{\sigma}_a} \right|$$

and unity otherwise. Generally γ may be taken as 1/2.

The coefficients of the polynomial which must pass through points A, B, and C can be readily determined from equations (A9). This is accomplished by replacing $\bar{\sigma}_{i3}$, $\bar{\sigma}_{i2}$, $\bar{\sigma}_{i1}$ by $\bar{\sigma}_A$, $\bar{\sigma}_B$, $\bar{\sigma}_C$, respectively, and $\bar{\varepsilon}_{i3}$, $\bar{\varepsilon}_{i2}$, $\bar{\varepsilon}_{i1}$ by $\bar{\varepsilon}_A$, $\bar{\varepsilon}_B$, $\bar{\varepsilon}_C$, respectively. The form of equation (A3) provides the strain-rate independent stress component, σ_s, on the appropriate path.

Reversal strain greater than upper cutoff strain: When the reversal strain, $\bar{\varepsilon}_A$, is greater than the upper cutoff strain, $\bar{\varepsilon}_U$, the positive path is approximated by a straight line segment of slope E_L equal to the secant slope of the previous negative path times a factor β which is chosen to agree with experimentally observed behavior.

Negative paths.- Negative paths are similar to the positive paths but employ a reversal strain, $\bar{\varepsilon}_{A'}$, when $\dot{\varepsilon}$ last changed sign from positive to negative and a lower cutoff strain, $\bar{\varepsilon}_L$. When a negative interior path intersects a negative envelope path, the envelope is followed.

Reversal strain less than lower cutoff strain: When the reversal strain, $\bar{\varepsilon}_{A'}$, is less than the lower cutoff strain, $\bar{\varepsilon}_L$, the negative path is approximated by a straight line of slope E_U equal to the secant slope of the previous positive path.

Reversal strain greater than lower cutoff strain: When the reversal strain, $\bar{\varepsilon}_{A'}$, is greater than the lower cutoff strain, $\bar{\varepsilon}_L$, the negative path is approximated by a fifth order polynomial similar to segment (4) but passing through three points designated as A', B', C' and with slope E_z at point C'. The relationships providing the state of stress-strain at these points may be found from equations (A10) through (A12) by replacing the subscripts A, B, C, $\bar{\sigma}_a$, and 3 by A', B', C', $\bar{\sigma}_b$, and 4, respectively. The coefficients of equations (A9) can then be evaluated from the resulting relationships, and then the form of equation (A3) provides the strain-rate independent stress components, $\bar{\sigma}_s$, on the appropriate path.

Cutoff strains, $\bar{\varepsilon}_U$ and $\bar{\varepsilon}_L$.- These strain values determine the regions of the enclosed envelope where straight line approximations are employed for positive and negative paths, respectively. Inasmuch as considerable computational time may be involved in creating polynomial path approximations each time the strain rate changes sign it can be advantageous to afford some loss in accuracy by using straight line approximations everywhere. By setting $\bar{\varepsilon}_U \leq \bar{\varepsilon}_{33}$ and $\bar{\varepsilon}_L \geq \bar{\varepsilon}_{53}$ only straight line approximations are used. On the

other hand, by setting $\bar{\varepsilon}_U = \bar{\varepsilon}_L = 0$ curved negative paths with straight line positive paths are used when $\bar{\varepsilon}_A > 0$ and curved positive paths with straight line negative paths are used when $\bar{\varepsilon}_A < 0$.

Additional restrictions: The tangent slope on any path may not exceed the maximum tangent slope on the envelope and must always be positive. In order to avoid poor curve fit approximations, $\bar{\varepsilon}_U$ should be less than $\bar{\varepsilon}_{51}$ and $\bar{\varepsilon}_L$ should be greater than $\bar{\varepsilon}_{61}$.

APPENDIX B

USER INSTRUCTIONS FOR DYNOTA (DYnamic NOnlinear Tile Analysis)

General Discussion

This appendix describes the user input and output of DYNOTA which is a computer program based on the uni-directional nonlinear dynamic tile/pad analysis in the main body of this paper. The program computes the response of the tile/pad system to sinusoidal and random imposed substrate motion and/or applied tile pressure.

Input Description

The program requires as input the number of cases to be executed, program control parameters, tile and pad geometry data, nonlinear viscous damping parameters, loading data, initial conditions, time step, and pad loading/unloading data. Following the first record which prescribes the number of cases to be executed, each case requires a minimum of 5 records and a maximum of 13 records as shown in figure 19.

The minimum 5 records are sufficient when the user wishes to take advantage of the standard loading/unloading pad property data built into the code and imposed substrate motions and applied tile pressures are sinusoidal in time. When imposed substrate motions and/or applied tile pressures are random one or two additional cards are required. If the standard pad data are not desired, the code allows for limited flexibility in adjusting these data by the use of a single additional record or complete flexibility by accepting user supplied pad property data on 5 additional records. A description of all records follows.

Record A1 - This record prescribes the number of cases to be executed as

NCASE

according to format I5.

Record B1 - This record prescribes control parameters

ISUB, IPRESS, MAXSTP, IRATE, IPRINT, IPLOT

according to format 6I5 where

ISUB = 0, no substrate motion
= 1, substrate motion

IPRESS = 0, no applied tile pressure
= 1, applied tile pressure

MAXSTP = total number of time steps

IRATE = 0, selects standard loading/unloading curve fit data for pad material properties without adjustment

= 1, expands or contracts the standard curve fit data parallel to the strain axis by a factor STRPER (defined on the D1 record) and moves the lower envelope of the standard data up by an amount DSTRS (defined on the D1 record)

= 2, user supplies loading/unloading curve fit data on records D2 through D6

IPRINT: Controls the values of time at which print output of pad strain, pad stress, rms stress, tile acceleration, substrate acceleration, and applied pressure are displayed

= 0, prints only at those times when pad stress is a relative maxima or minima

= 1, prints every time step

= N, prints every Nth time step

IPLOT: Controls output plots

= 0, no plots

= 1, generates the following plots for random response:

(a) Imposed random substrate acceleration versus time

(b) Applied random tile pressure versus time

(c) Tile response acceleration versus time

= 2, same as IPLOT = 1 but for pure sinusoidal imposed substrate motion and applied tile pressure

= 3, plots out the stress-strain curves being traced during entire period of case execution

Record B2 - This record prescribes file and pad properties as

AREAP, AREAT, THICK, SM, GAMMA, BETA, CUTOFF1, CUTOFF2

according to format 8E10.4 where

AREAP = contact area between pad and tile

AREAT = surface area of tile on which pressure acts

THICK = pad thickness after conditioning

SM = tile mass

GAMMA = low stress loading/unloading factor, see equation (A11) (Default: 1/2)

BETA = multiplying factor for straight line loading/unloading interior paths as described in Appendix A (Default: 2)

CUTOFF1 = $\bar{\varepsilon}_U$, see Appendix A (Default: $\bar{\varepsilon}_{51}$)

CUTOFF2 = $\bar{\varepsilon}_L$, see Appendix A (Default: $\bar{\varepsilon}_{61}$)

Record B3 - This record prescribes pad damping properties as

DAMP, QM

according to format 2E12.5 where

DAMP = ζ (Default: 0.15)

QM = q (Default: 2)

Record B4 - This record prescribes applied substrate motion and tile pressure

AMPS, FREQS, AMPP1, AMPP2, FREQP, GRAV

according to format 6E10.4 where

AMPS = α = dimensionless amplitude of sinusoidal substrate acceleration in multiples of G

FREQS = $\Omega/2\pi$ = circular frequency of sinusoidal substrate acceleration (Hz)

AMPP1 = p_1 = amplitude of nonoscillatory component of applied pressure

AMPP2 = p_2 = amplitude of sinusoidal component of applied tile pressure

FREQP = $\omega/2\pi$ = circular frequency of sinusoidal component of applied tile pressure

GRAV = G = gravitational constant (Default: G = 386 in/sec^2)

Note for Random Response:

FREQS and/or FREQP set to zero implies imposed random substrate acceleration and/or applied random tile pressure, respectively, read from binary

tapes, TAPE1 and/or TAPE2, respectively. Each record contains one data entry.

Record B5 - This record prescribes initial conditions and time step as

SIG, EPS, EPSD, DT

according to format 4E10.4 where

SIG = initial pad stress

EPS = initial pad strain

EPSD = initial tile strain rate

DT = time step, Δt

Record C1 - This record is used only when ISUB = 1 and FREQS = 0 to prescribe specifications on imposed substrate acceleration histories on TAPE1 as

NR1, NS1, TINC1, SCALE1

according to format 2I5, 2E10.4 where

NR1 = total number of records on TAPE1

NS1 = number of records at start of TAPE1 to be skipped

TINC1 = uniform time increment between records on TAPE1

SCALE1 = scale factor to be applied to TAPE1 data

Record C2 - This record is used only when IPRESS = 1 and FREQP = 0 to prescribe specifications on applied tile pressure histories on TAPE2 as

NR2, NS2, TINC2, SCALE2

according to format 2I5, 2E10.4 where

NR2 = total number of records on TAPE2

NS2 = number of records at start of TAPE2 to be skipped

TINC2 = uniform time increment between records of TAPE 2

SCALE2 = scale factor to be applied to TAPE2 data

Record D1 - This record is used only when IRATE = 1 on the B1 record and prescribes adjustments to the standard loading/unloading pad property data as

STRPER, DSTRS

according to format 2E10.4. See description under IRATE = 1 on B1 record for definitions.

Records D2-D6 - These five records are used only when IRATE = 2 on the B1 record to prescribe user supplied loading/unloading pad property data according to the formulation of Appendix A (illustrated in figure 19). These records have the form

$\bar{\sigma}_a$, $\bar{\sigma}_b$, E_z ; record D2

$\bar{\varepsilon}_{31}$, $\bar{\varepsilon}_{32}$, $\bar{\varepsilon}_{33}$, $\bar{\sigma}_{32}$, $\bar{\sigma}_{33}$; record D3

$\bar{\varepsilon}_{41}$, $\bar{\varepsilon}_{42}$, $\bar{\varepsilon}_{43}$, $\bar{\sigma}_{42}$, $\bar{\sigma}_{43}$; record D4

$\bar{\varepsilon}_{51}$, $\bar{\varepsilon}_{52}$, $\bar{\sigma}_{52}$; record D5

$\bar{\varepsilon}_{61}$, $\bar{\varepsilon}_{62}$, $\bar{\sigma}_{62}$; record D6

each according to format 5E10.4

Output Description

Program displays at user selected times pad through-the-thickness stress and strain, tile acceleration, substrate acceleration, and applied pressure. Also displayed are rms stress, tile acceleration, and imposed substrate acceleration. In addition, the program assembles necessary arrays of data for post-processing. The user may use these arrays in conjunction with post-processing routines such as those which compute power spectral density. Such routines are generally available in the program library of most computer centers.

REFERENCES

1. Sawyer, J. W.; and Rummler, D. R.: Room Temperature Mechanical Properties of Shuttle Thermal Protection System Materials. NASA TM-81786, April 1980.

2. Housner, J. M.; and Garcia, R.: Nonlinear Static TPS Analysis. NASA TM-81785, March 1980.

3. Timoshenko, S.: Vibration Problems in Engineering. D. Van Nostrand Co., Inc., N.Y., 2nd edition, 1937, pp. 57-61 and 32-37.

4. Richardson, P. D.: Natural Vibration With Damping Proportional to a Power of the Velocity. Journal of the Royal Aeronautical Society, Vol. 68, Dec. 1964, pp. 846-849.

5. Miserentino, R.; Pinson, L. D.; and Leadbetter, S. A.: Some Space Shuttle Tile/Strain-Isolator-Pad Sinusoidal Vibration Tests. NASA TM-81853, July 1980.

6. Miserentino, R.; Pinson, L. D.; and Leadbetter, S. A.: Some Vibration Characteristics of a Space Shuttle Tile/Strain-Isolator-Pad System. Presented at the 1980 SAE Aerospace and Exposition, Oct. 13-16, 1980, Los Angeles, CA.

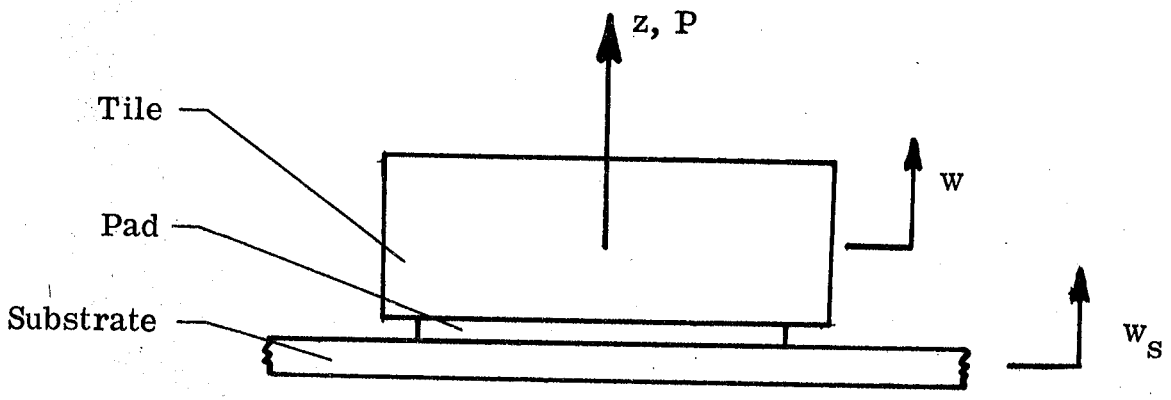

Figure 1.- Tile pad and geometry.

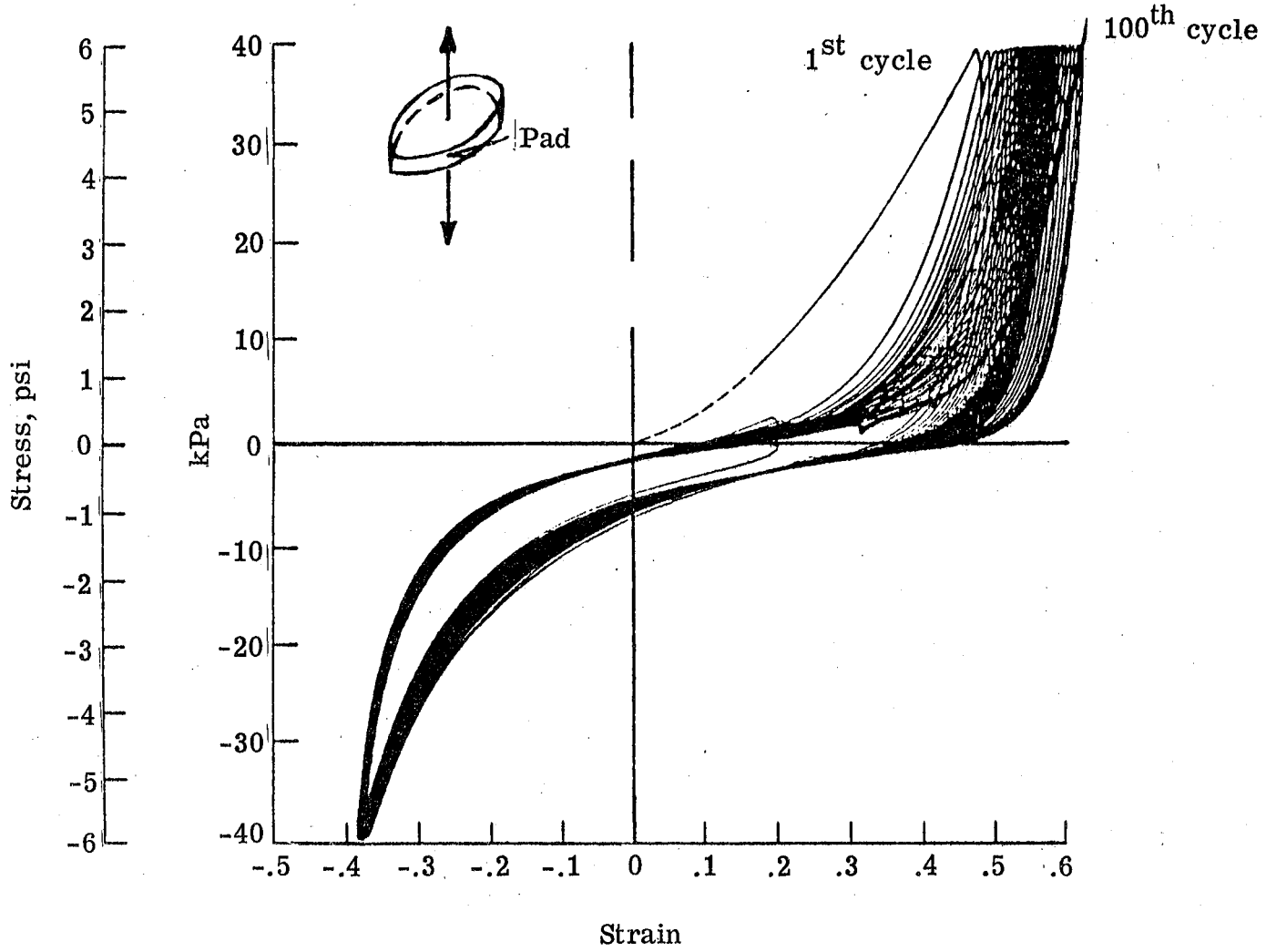

Figure 2.- Nonlinear behavior of pad illustrating the effect of cyclic loading on through-the-thickness stress, [pad thickness = .406 cm (.160 in.)]

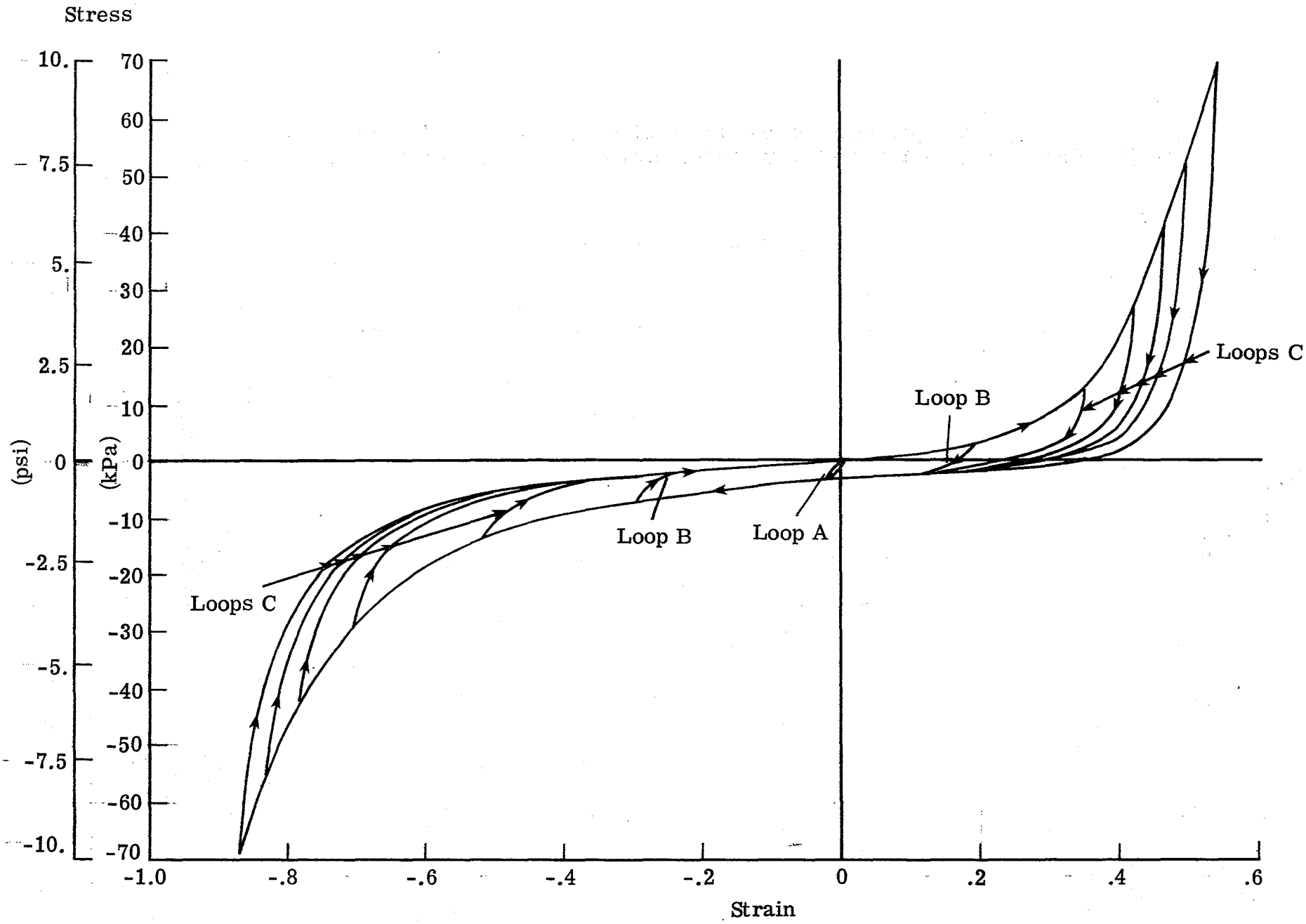

Figure 3.- Loading/unloading paths within a conditioned hysteretic envelope
[pad thickness = 0.406 cm (.106 in.)]

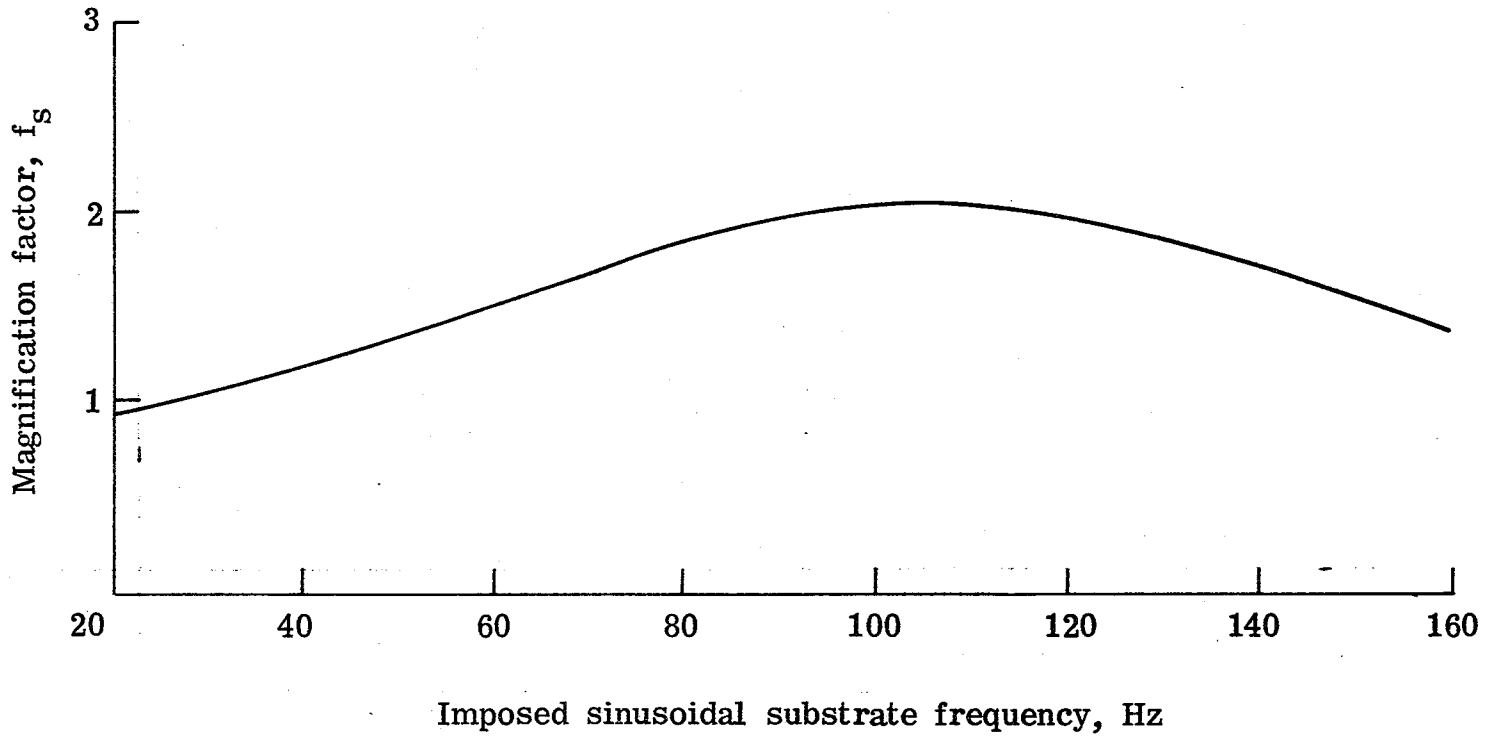

Figure 4.- Typical variation of magnification factor with imposed sinusoidal substrate frequency for a prescribed substrate acceleration amplitude, $\alpha = 10$, ($q = 2$, $\zeta = .15$).

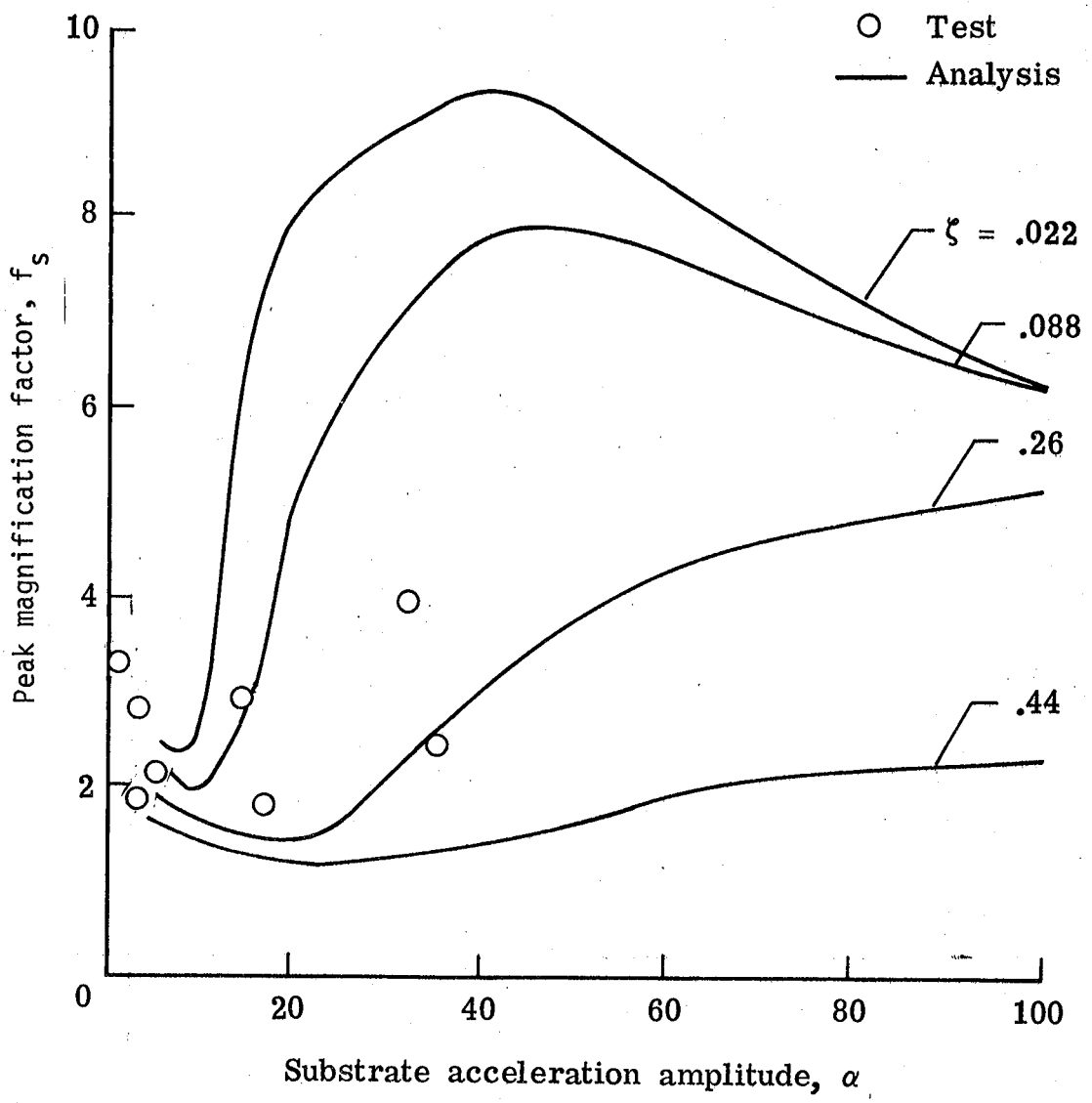

Figure 5.- Effect of nonlinear viscous damping parameter, ζ, on magnification factor when q = 1., Ω_r=100 Hz.

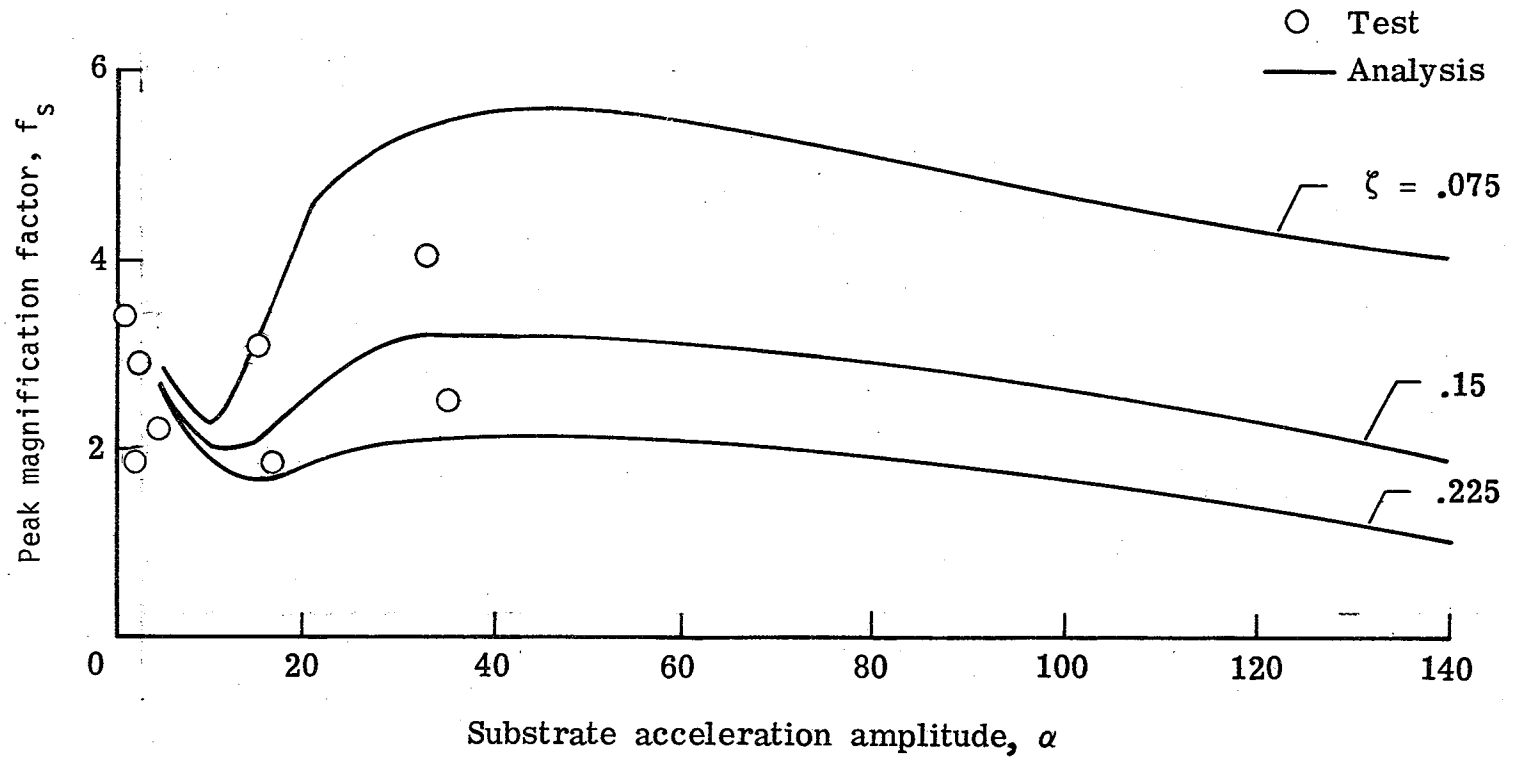

Figure 6.- Effect of nonlinear viscous damping parameter, ζ, on magnification factor when $q = 2$, Ω_r=100 Hz.

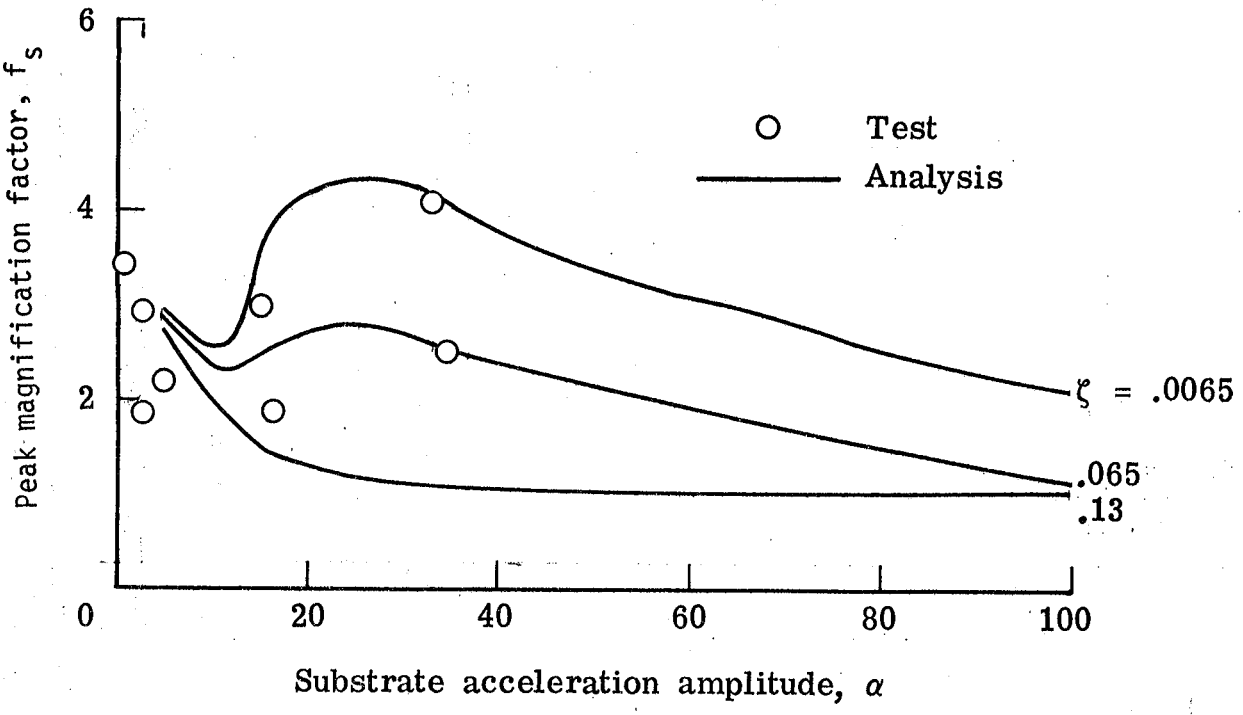

Figure 7.- Effect of nonlinear viscous damping parameter, ζ, on magnification factor when q = 3, Ω_r=100 Hz.

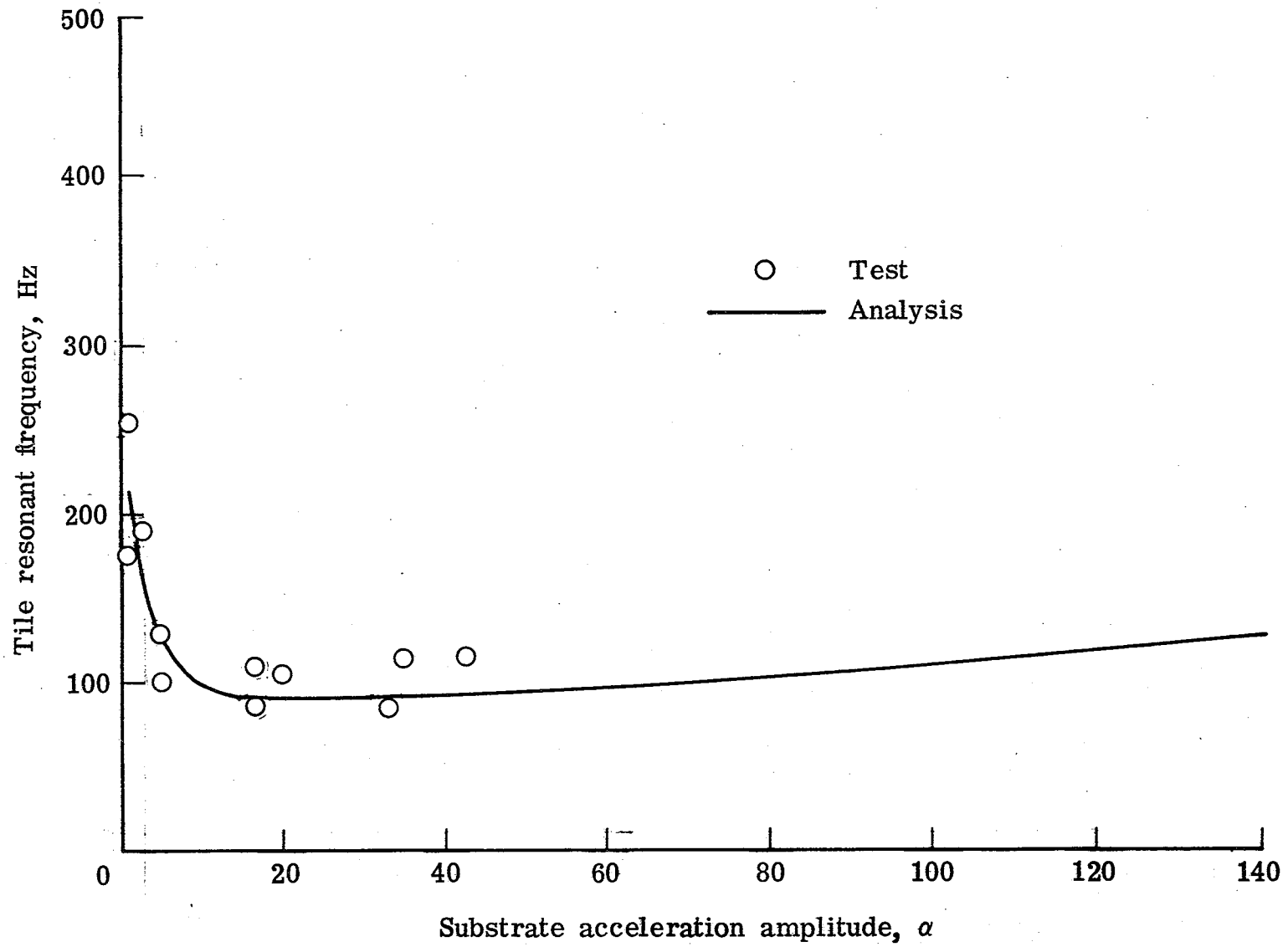

Figure 8.- Variation of tile resonant frequency with imposed sinusoidal substrate acceleration amplitude, ($q = 2$, $\zeta = .15$).

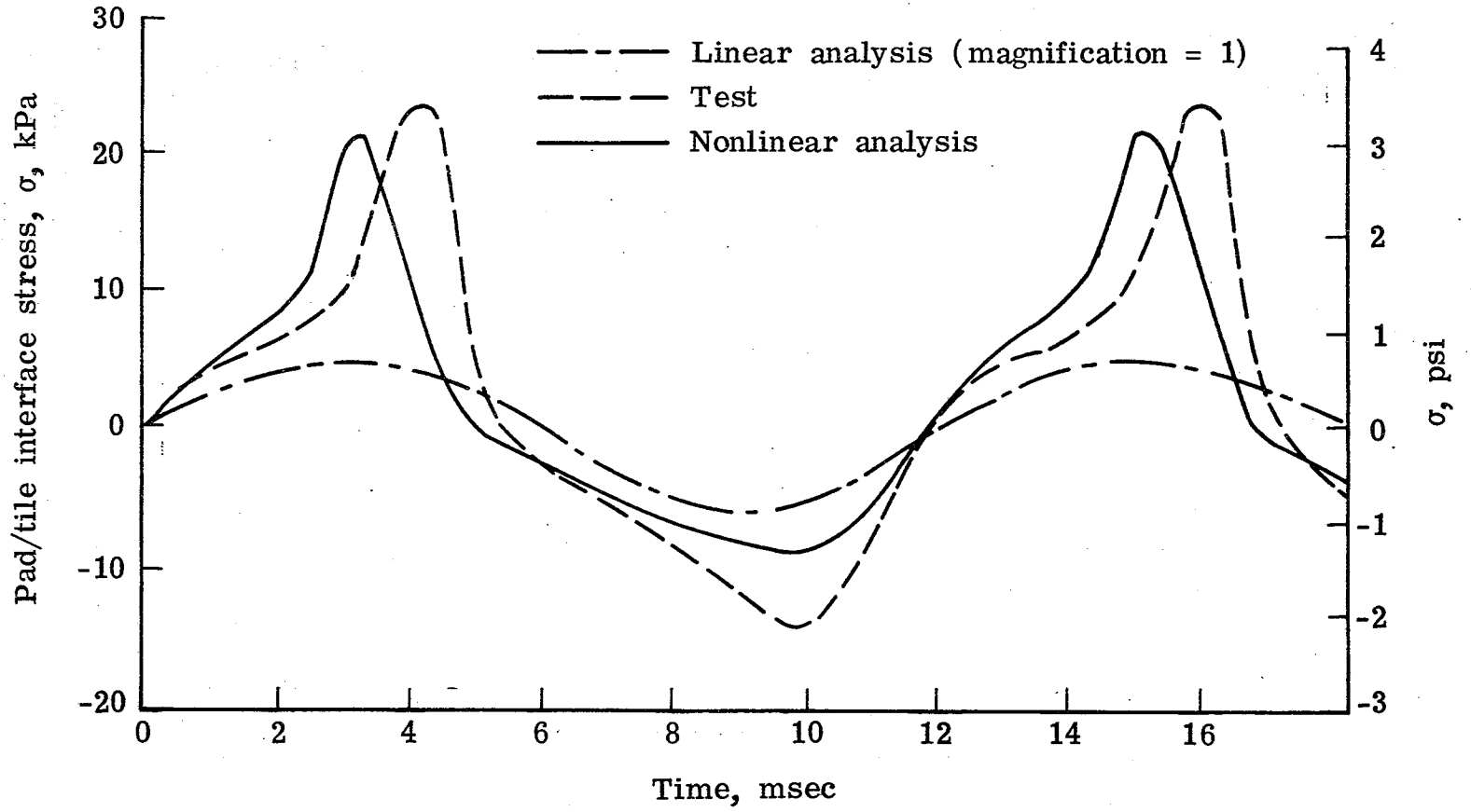

Figure 9.- Nonlinear wave shape due to sinusoidal substrate acceleration, α = 30.

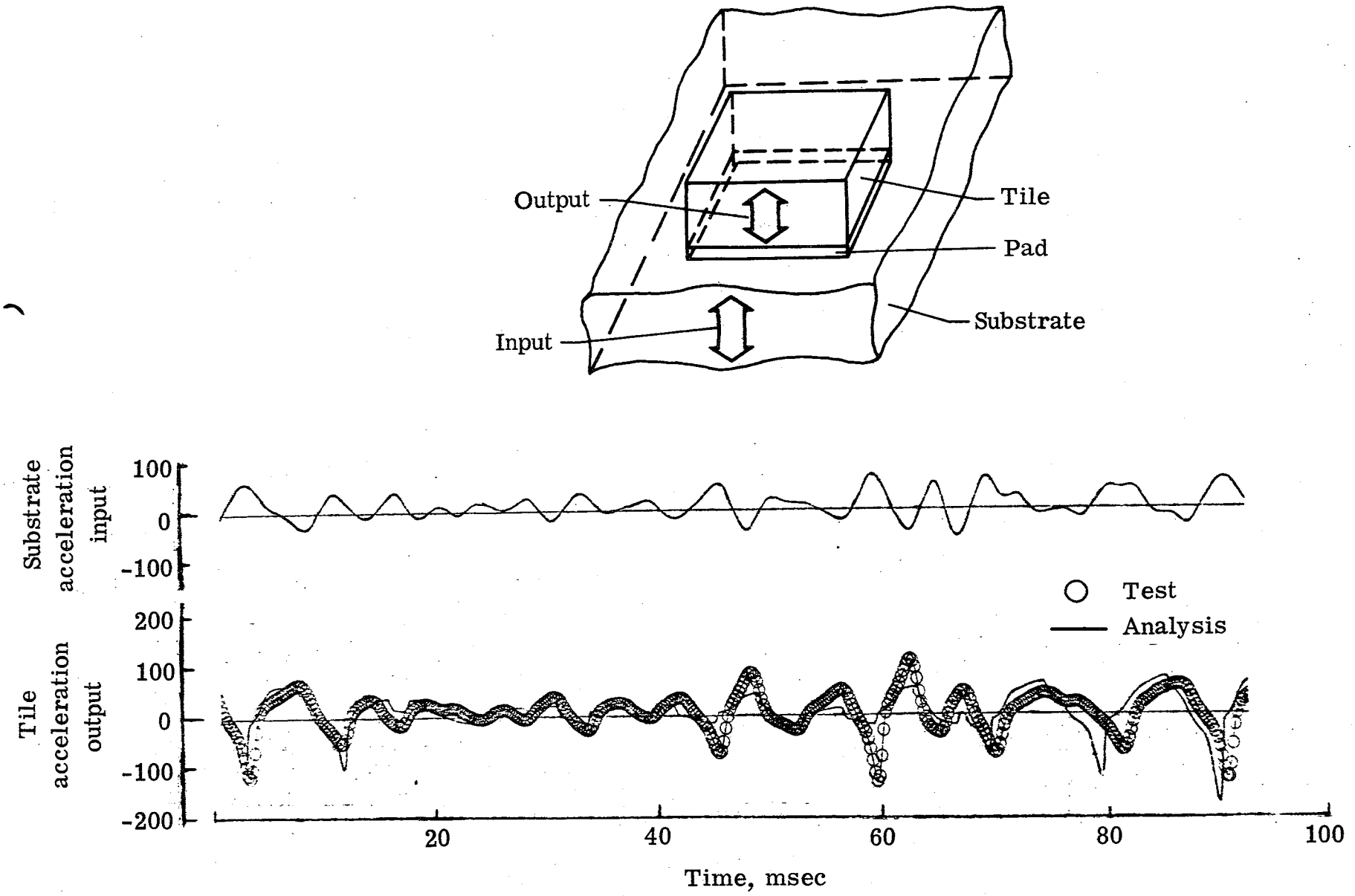

Figure 10.- Tile response to random substrate acceleration.

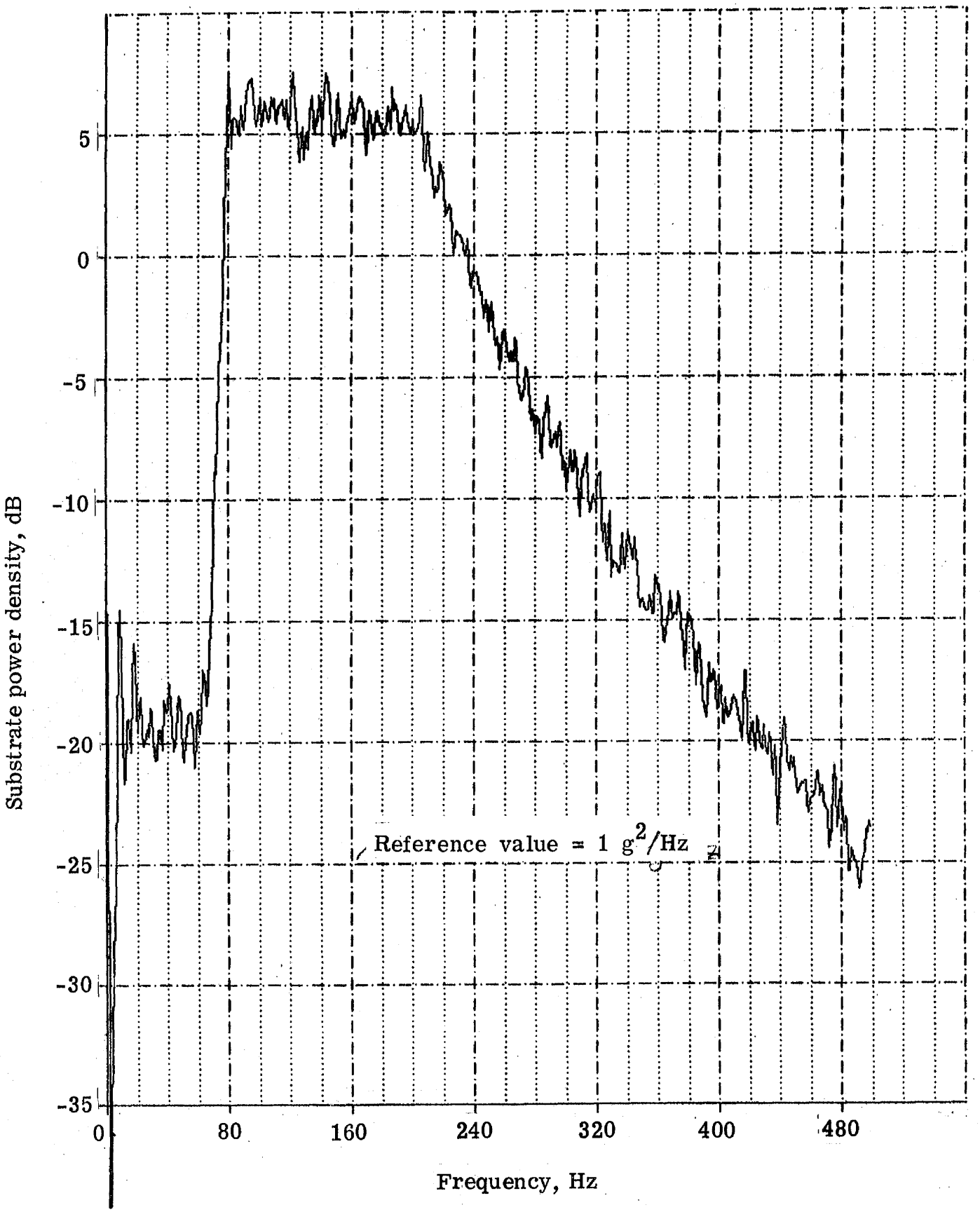

Figure 11.- Power spectral density of imposed random substrate acceleration.

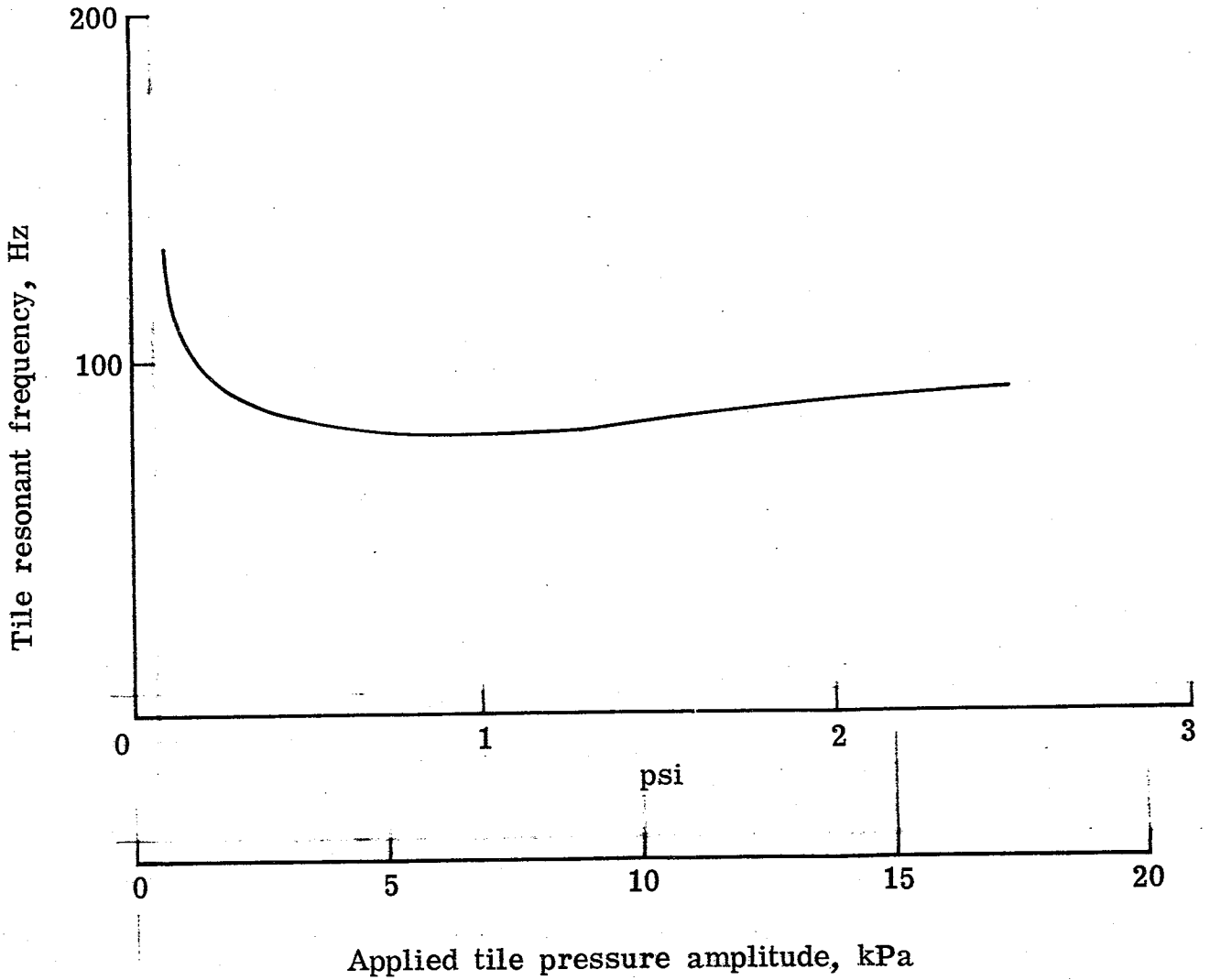

Figure 12.- Variation of resonant tile frequency with applied sinusoidal tile pressure amplitude, ($q = 2$, $\zeta = .15$).

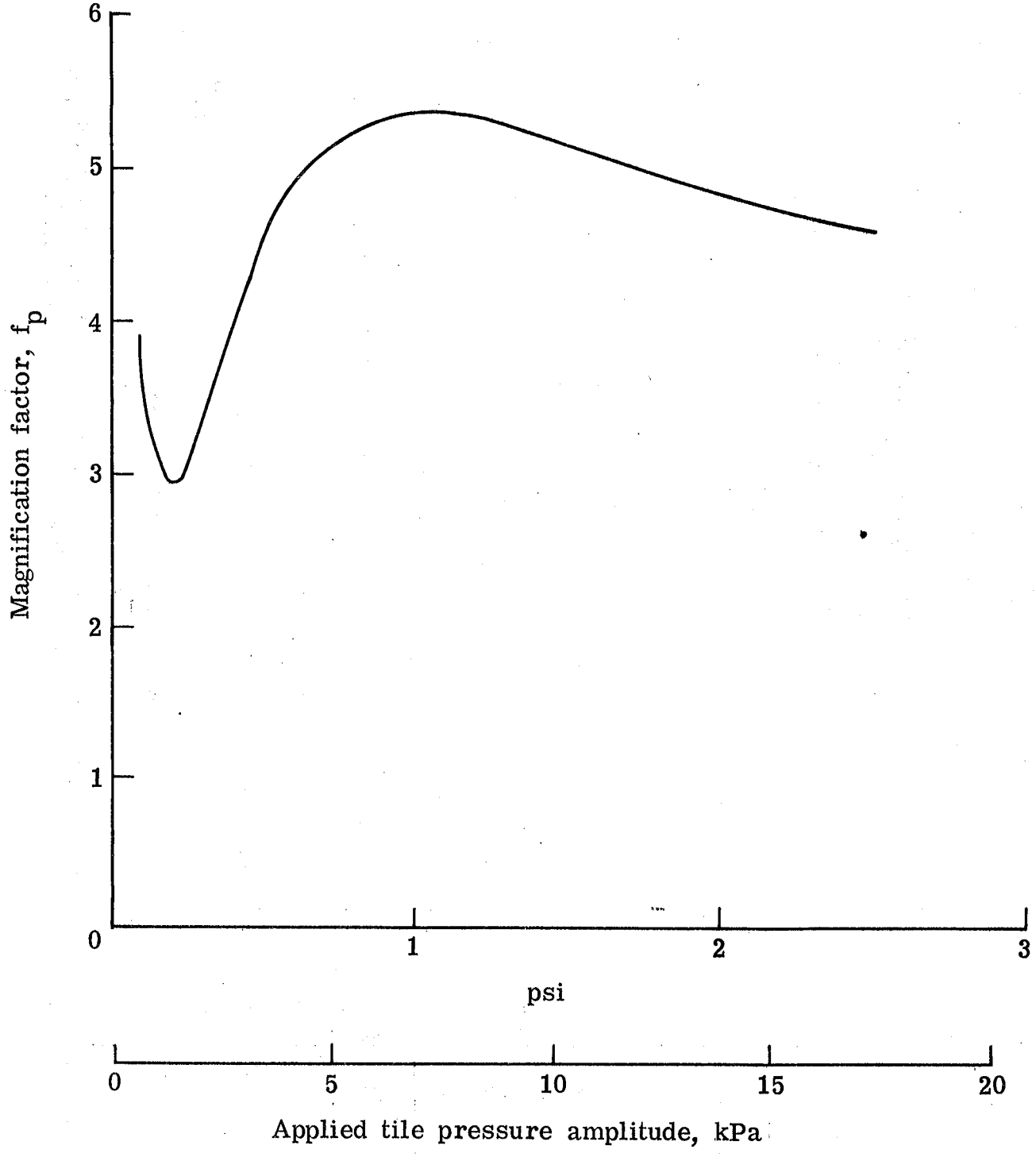

Figure 13.- Variation of magnification factor with applied sinusoidal tile pressure amplitude, ($q = 2$, $\zeta = .15$).

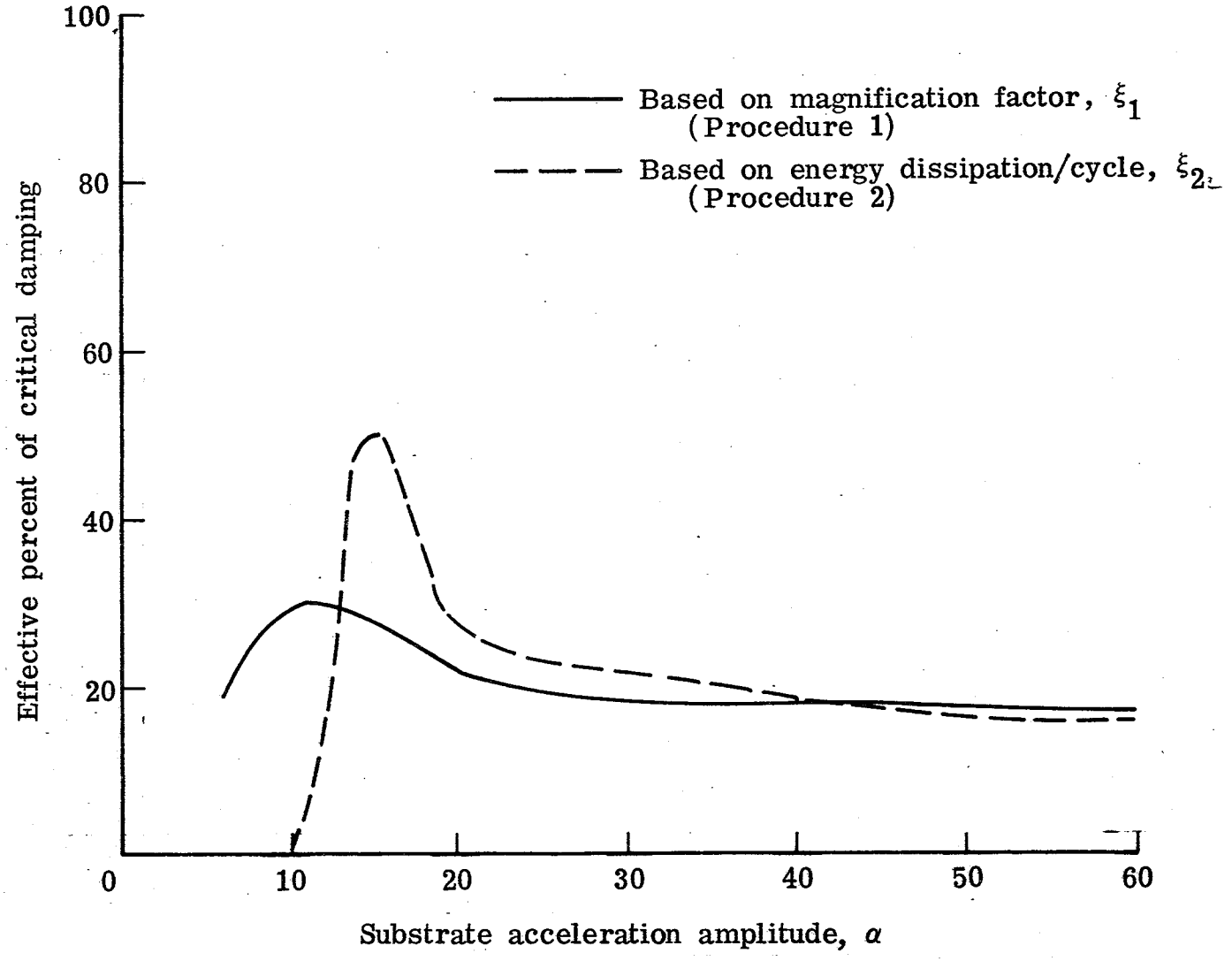

Figure 14.- Effective percent of critical damping on the basis of magnification factor and energy dissipation/cycle under imposed sinusoidal substrate acceleration.

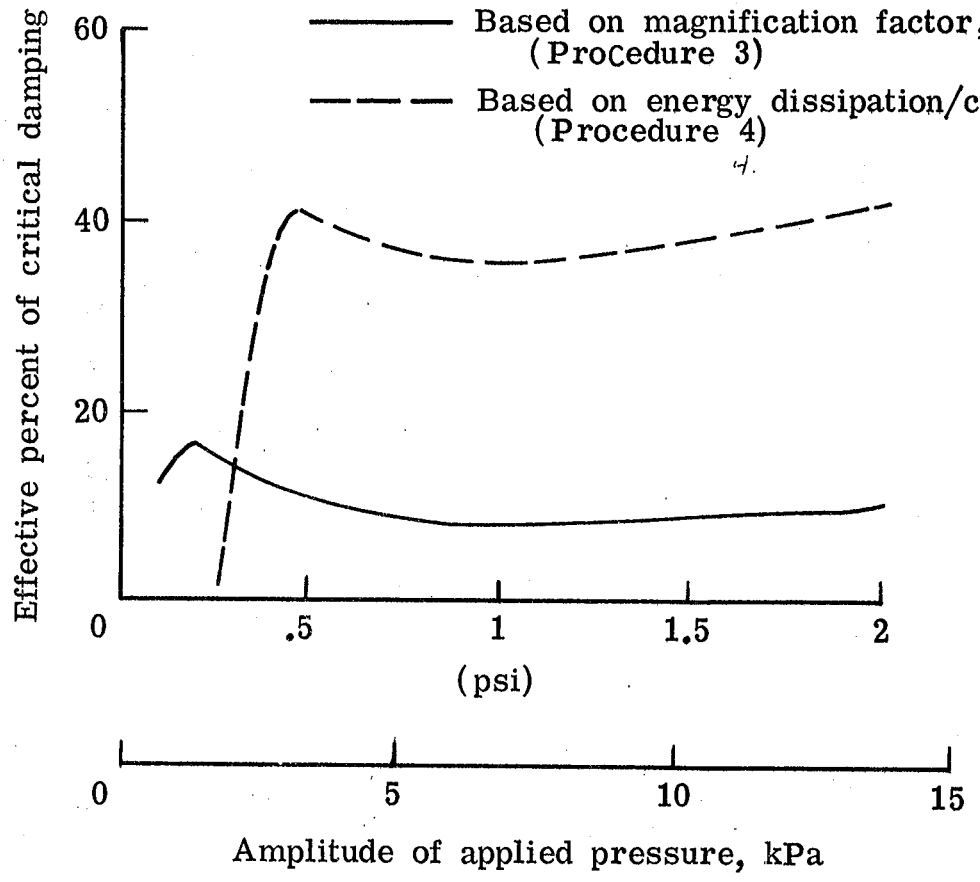

Figure 15.- Effective percent of critical damping on the basis of magnification factor and energy dissipation/cycle under applied sinusoidal tile pressure.

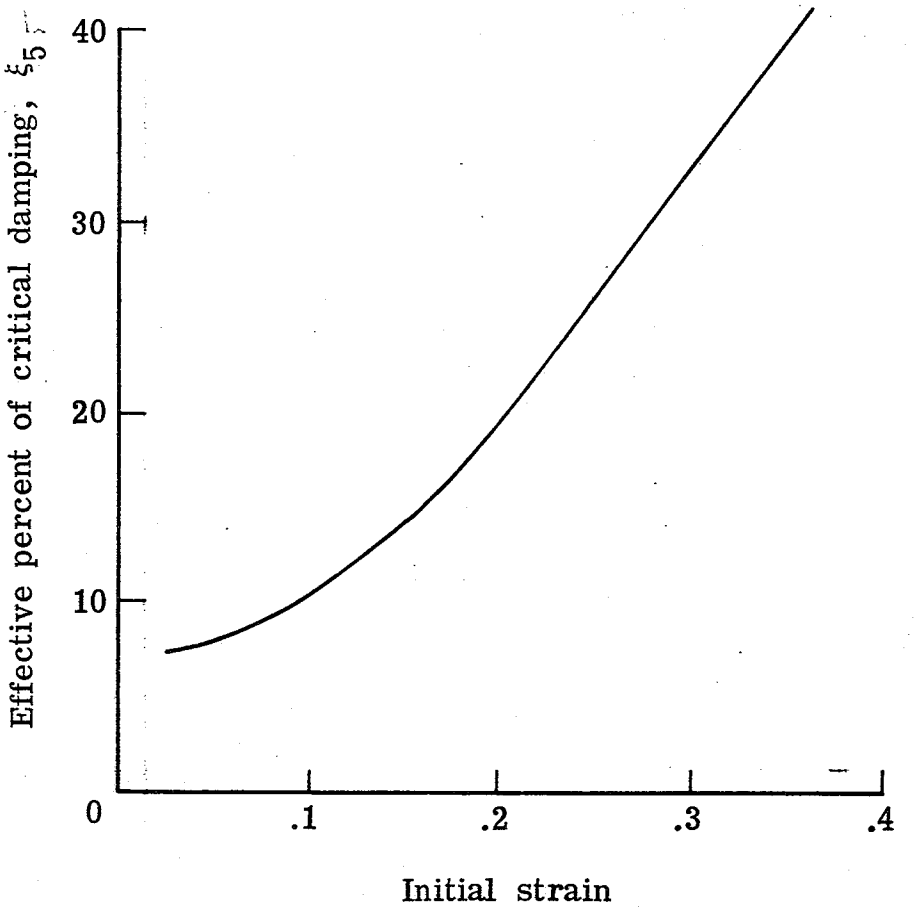

Figure 16.- Effective percent of critical damping on the basis of log decrement, procedure 5.

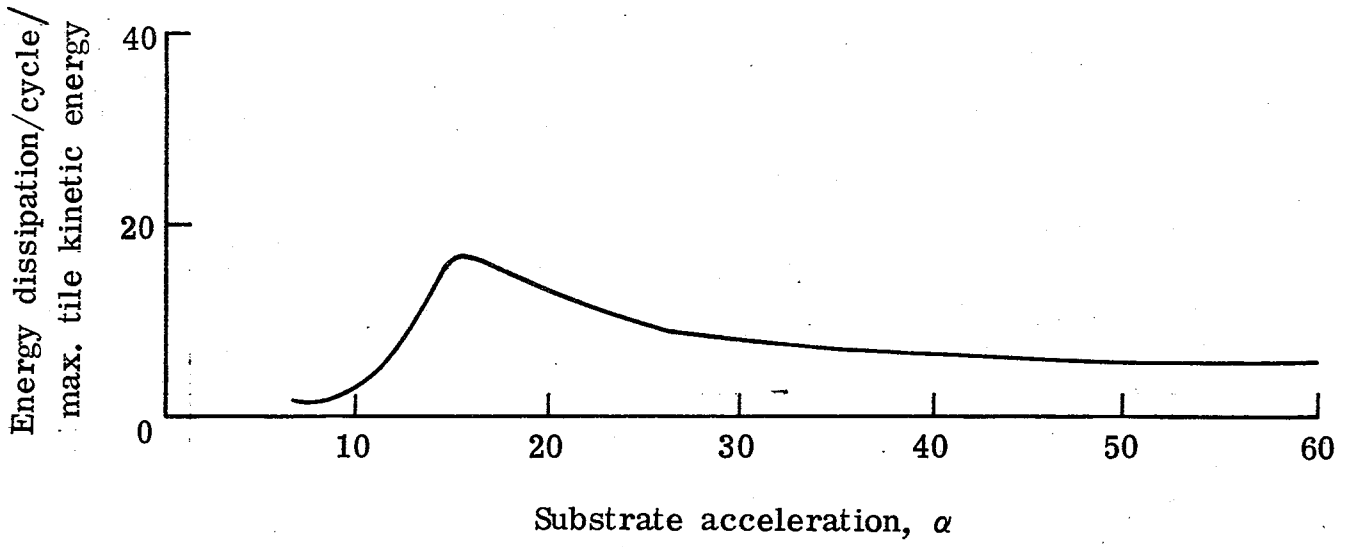

Figure 17.- Energy dissipation/cycle due to frictional damping under imposed sinusoidal substrate acceleration.

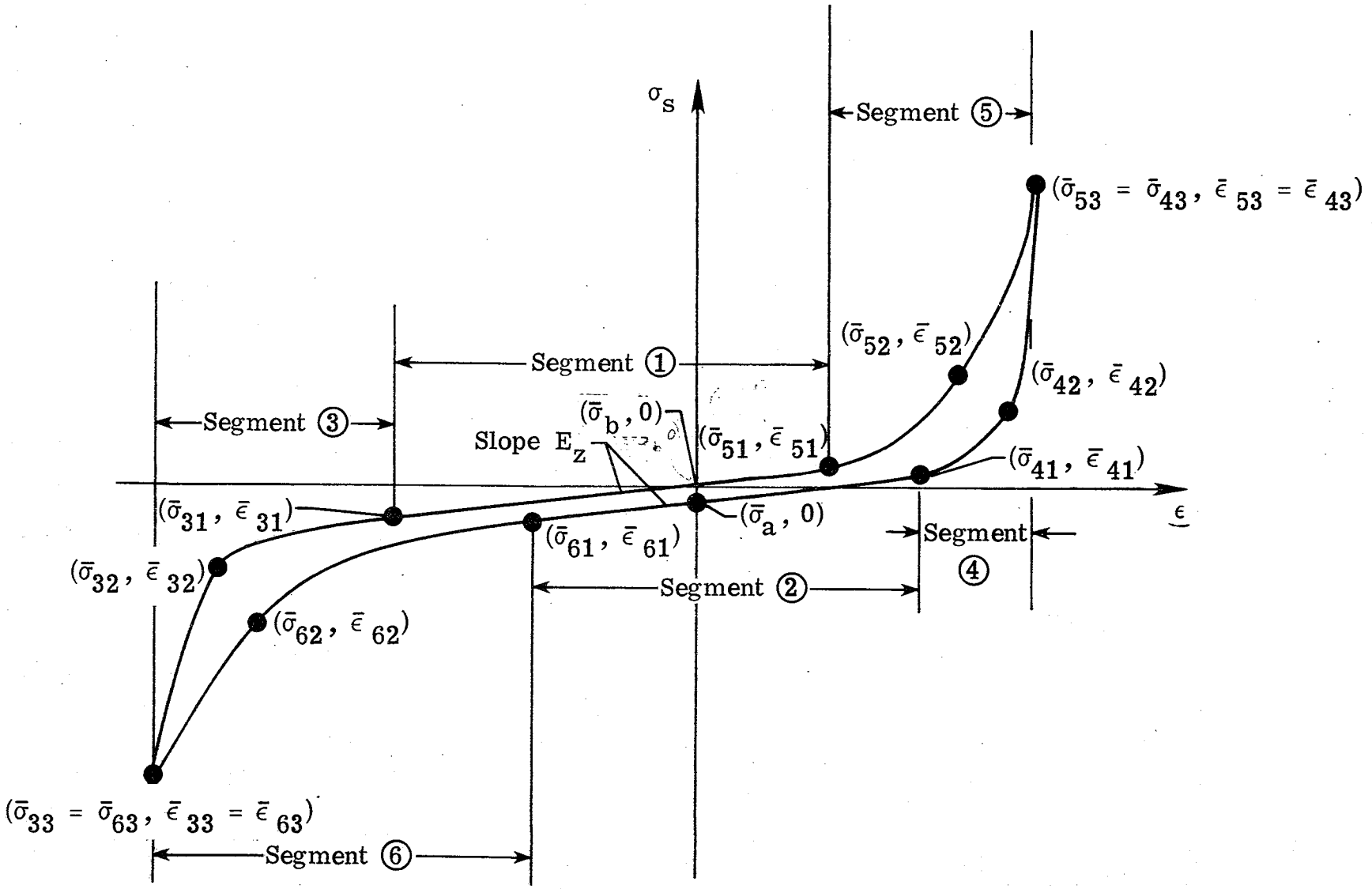

Figure 18.- Curve fit for strain-rate independent loading/unloading path envelope.

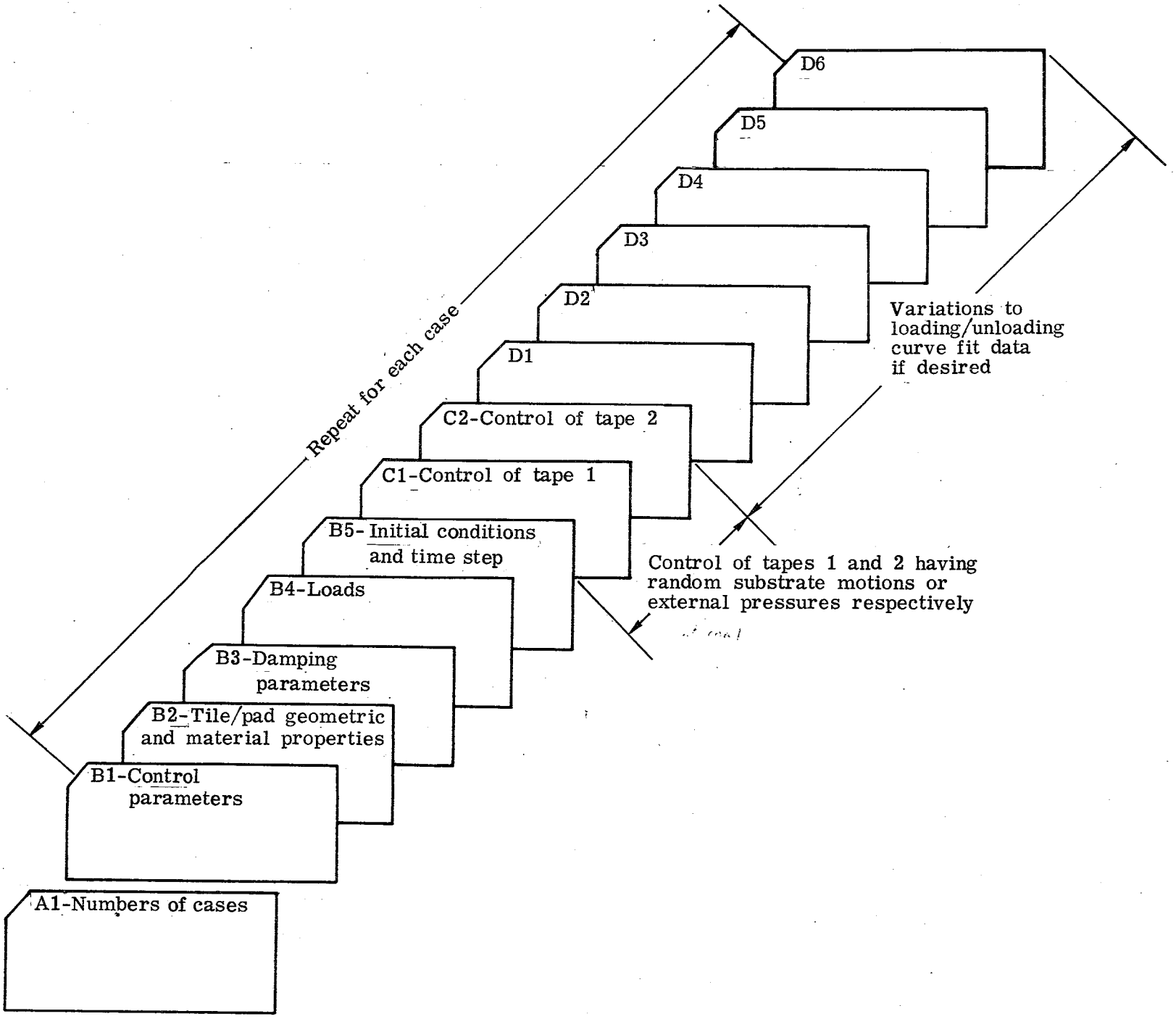

Figure 19.- Schematic of input data deck.

1. Report No.	2. Government Accession No.	3. Recipient's Catalog No.
NASA TM-81901		

4. Title and Subtitle	5. Report Date
Nonlinear Dynamic Response of a Uni-Directional Model for the Tile/Pad Space Shuttle Thermal Protection System	November 1980
	6. Performing Organization Code
7. Author(s)	8. Performing Organization Report No.
Jerrold M. Housner, *Harold H. Edighoffer, and **K. C. Park	
9. Performing Organization Name and Address	10. Work Unit No.
NASA Langley Research Center Hampton, VA 23665	11. Contract or Grant No.
12. Sponsoring Agency Name and Address	13. Type of Report and Period Covered
National Aeronautics and Space Administration Washington, DC 20546	Technical Memorandum
	14. Sponsoring Agency Code

15. Supplementary Notes

*General Electric Company, Philadelphia, Pennsylvania 19101
**Lockheed Palo Alto Research Laboratories, Palo Alto, California 94304

16. Abstract

A uni-directional analysis of the nonlinear dynamic behavior of the space shuttle tile/pad thermal protection system is developed and examined for imposed sinusoidal and random motions of the shuttle skin and/or applied tile pressure. The analysis accounts for the highly nonlinear stiffening hysteresis and viscous behavior of the pad which joins the tile to the shuttle skin. Where available, experimental data are used to confirm the validity of the analysis. Both analytical and experimental studies reveal that the system resonant frequency is very high for low amplitude oscillations but decreases rapidly to a minimum value with increasing amplitude. Analytical studies indicate that with still higher amplitude the resonant frequency increases slowly. The nonlinear pad is also responsible for the analytically and experimentally observed distorted response wave shapes having high sharp peaks when the system is subject to sinusoidal loads. Furthermore, energy dissipation in the pad is studied analytically and it is found that the energy dissipated is sufficiently high to cause rapid decay of dynamic transients. Nevertheless, the sharp peaked nonlinear responses of the system lead to higher magnification factors than would be expected in such a highly damped linear system.

17. Key Words (Suggested by Author(s))	18. Distribution Statement
space, shuttle, nonlinear dynamic response	Unclassified - Unlimited Subject Category 39

19. Security Classif. (of this report)	20. Security Classif. (of this page)	21. No. of Pages	22. Price*
Unclassified	Unclassified	42	A03

For sale by the National Technical Information Service, Springfield, Virginia 22161